Description of the software Heliosat-2 for the conversion of images acquired by Meteosat satellites in the visible band into maps of solar radiation available at ground level

Mireille Lefèvre, Michel Albuisson, Lucien Wald

▶ To cite this version:

DESCRIPTION OF THE SOFTWARE HELIOSAT-II

FOR THE CONVERSION OF IMAGES ACQUIRED BY METEOSAT

SATELLITES IN THE VISIBLE BAND INTO MAPS OF SOLAR

RADIATION AVAILABLE AT GROUND LEVEL

M. Lefèvre, M. Albuisson, L. Wald

November 2002

First Revision: February 2004

Heliosat Web site: http://www.helioclim.org/heliosat

Abstract

This document describes the software Heliosat-II developed by the Groupe Télédétection & Modélisation, Centre d'Energétique, a joint research unit of Armines and Ecole des Mines de Paris.

The method Heliosat-II was developed by this research group in 2000-2001, partly with the support of the European Commission (project SoDa, contract DG "INFSO" IST-1999-12245, http://www.soda-is.com).

This method converts images acquired by the satellite Meteosat into maps of global irradiation received at ground level. Under concern are the images acquired in the visible band of the Meteosat sensor.

The software was developed in C for a Unix station.

The present document describes the various libraries and procedures. It describes how these can be implemented for the correct execution of the whole method. The procedures described here comprise I/O orders that are to be tailored to the specific format for Meteosat images.

The method can be applied to other geostationary satellites offering similar broadband in the visible range (0.4 – 1.1 μm). The input images are geometrically superimposable images. Calibration coefficients exist that convert digital counts into radiances (W m^{-2} sr^{-1}).

These codes can be downloaded at the Heliosat Web site: http://www.helioclim.org/heliosat.

Revisions

February 2004: the definition of the angle $\boldsymbol{q}_v$ is better expressed (section2.5).

Table of Contents

1.   Introduction

This document describes the software Heliosat-II developed by the Groupe Télédétection & Modélisation, Centre d'Energétique, a joint research unit of Armines and Ecole des Mines de Paris.

The method Heliosat-II was developed by this research group in 2000-2001, partly with the support of the European Commission (project SoDa, contract DG "INFSO" IST-1999-12245, http://www.soda-is.com).

This method converts images acquired by the satellite Meteosat into maps of global irradiation received at ground level. Under concern are the images acquired in the visible band of the Meteosat sensor. It was proved that the method Heliosat-II provides better results than its state-of-the-art counterparts do. The accuracy was assessed by the means of a comparison with measurements made in the meteorological network in Europe.

The software was developed in C for a Unix station.

The present document describes the various libraries and procedures. It describes how these can be implemented for the correct execution of the whole method. The procedures described here comprise I/O orders that should not be used as such but should be tailored to the specific formats used by the user for Meteosat images and other data.

The method can be applied to other geostationary satellites offering similar broadband in the visible range (0.4 – 1.1 µm). The input images are geometrically superimposable. Calibration coefficients exist that convert digital counts into radiances (W m^{-2} sr^{-1}).

These codes can be downloaded at the Heliosat Web site: http://www.helioclim.org/heliosat.

What is the accuracy of the method?

We made comparisons between satellite-derived assessments and measurements performed in the world radiation network in Europe and Africa. The results depend upon several parameters; the type of data (high-resolution or B2 format) and the number of pixels whose values are averaged for the comparison with the irradiation measurements. The following table reports the RMSE (root mean square error) observed for several parameters for irradiation and irradiance. The comparison was made for a single pixel (that containing the station) and for 30 stations WMO in Europe, outside mountainous areas. Averaging over several pixels is the standard procedure used by most researchers, e.g. 5x5 or more. It reduces the RMSE, leaving the bias unchanged.

Type	*Irradiation (Wh m^{-2})*	*Type*	*Irradiance (W m^{-2})*
Hourly values	100	Hourly average	100
Daily values	600	Daily average	25
5-days sum of daily irradiation	2500	5-days average	20
10-days sum of daily irradiation	3500	10-days average	15
Monthly mean of hourly irradiation	50	Monthly mean for a given hour	50
Monthly mean of daily irradiation	300	Monthly mean	12

Typical accuracy values expressed as RMSE for irradiation (Wh m^{-2}) and irradiance (W m^{-2}) reached by the method Heliosat-II. Comparison was made for a single pixel and for 30 stations WMO in Europe

The following table shows the bias and RMSE observed when comparing irradiances obtained by the method Heliosat-II and those measured by 60 stations WMO in Europe and 30 in Africa for one year (Lefèvre *et al.* 2002). Irradiances are derived from monthly means. This comparison was made for

single pixel (5' of arc angle in size, approx. 10 km at mid-latitude) and also for cell of 0.5° in size. It shows how the RMSE decreases when data are spatially averaged.

The bias and root mean square error (RMSE) for the assessment of the irradiance for a month are equal to respectively 2 and 11 W m^{-2} on small cells. The RMSE may decrease down to 4 W m^{-2} if assessments are averaged over cells of 0.5° of arc angle.

The performances are worse for the data in the reduced-resolution B2 format. This format results from a sub-sampling of the high-resolution data. Briefly written, one pixel out of six original pixels is kept. Estimates at the geographical locations of the stations are therefore produced by spatial interpolation of the irradiation assessed for each of the nine closest cells. The distance used is that of Lefevre *et al.* (2002). To the inherent error of the method Heliosat-II, is added the interpolation error. Comparisons were performed using 60 stations in Europe and 30 stations in Africa for the same year. The bias and RMSE are better than respectively 3 and 17 W m^{-2} for one month and a cell of 5'. The RMSE decreases to 9 W m^{-2} for cells of 0.5° in size.

	Hi-Res images		*B2 format*	
	5' cell	0.5° cell	5' cell	0.5° cell
Bias	2	2	3	3
RMSE	11	4	17	9

Errors (W m^{-2}) in assessing SW downward irradiance for a month. In Lefevre et al. (2002)

2. <u>Nomenclature</u>

The following notations are employed in this document.

The following subscripts are used

- *0*: extraterrestrial or astronomical values,

- *g*: ground related values,

- *c*: clear sky (*i.e.* cloudless sky) values,

- *b*: overcast sky values.

- *l*: spectral values.

2.1. Astronomical quantities and sun angles

- *t* is the time.

- q_S is the sun zenithal angle.

- g_s is the sun elevation at time *t*, also called the solar altitude angle. g_s is 0° at sunrise and sunset. $q_S = p/2 - g_S$.

- *a* is the sun azimuth angle.

- I_0 is the solar constant, that is the extraterrestrial irradiance normal to the solar beam at the mean solar distance. It is equal to 1367 W.m^{-2}.

- I_{0l} is the spectral distribution of solar radiation outside the atmosphere. It is created by averaging or interpolating values read in published tables, to irradiance for 10 nm intervals centred on the indicated wavelengths. These tables are those of Neckel, Labs (1984), read from Justus (1989) and Rossow *et al.* (1992). Units are W m^{-2} μm^{-1}.

- *e* is the correction used to allow for the variation of sun-earth distance from its mean value. It depends upon the day. I_0 *e(t)* is the extraterrestrial irradiance for the current day observed on a surface normal to the solar beam.

- *d* is the declination (positive when the sun is north to the equator: March 21 to September 23). Maximum and minimum values of the declination are +23°27' and -23°27'.

- *Dl* is the length of the day, *i.e.* 24 hours or 86400 seconds.

- the solar hour angle, *w*, expresses the time of the day in terms of the angle of rotation of the Earth about its axis from its solar noon position at a specific place. As the Earth rotates of 360° (or 2π rad) in 24 hours, in one hour the rotation is 15° (or π/12 rad). Given an instant *t* in true solar time (TST) expressed in decimal hour, *w = (t-12)p/12*. If *t* is Universal Time (UT) in decimal hour, if *l* is the longitude (positive eastwards) and if *Dt* is the correction of time (the so-called equation of time) in decimal hour, then *w = p/12 (t + 12l/p + Dt – 12)*, if *l* is in radians, or *w = 15 (t + l/15 + Dt – 12)* if *l* is expressed in degrees.

- w_{SR} and w_{SS} are the solar hour angles at respectively sunrise and sunset.

2.2. Radiation quantities

The letters *L*, *G*, *D*, *I* and *B* denote the following quantities:

- *L*: radiance (W m^{-2} sr^{-1}),

- *G*: global irradiance or irradiation,

- *D*: diffuse irradiance or irradiation (diffuse component of solar radiation),

- *I*: normal direct irradiance or irradiation (beam component of solar radiation normal to the direction of the sun),

- *B*: direct irradiance or irradiation (beam component of solar radiation).

The basic time intervals to which the irradiation values refer are identified by the following subscripts:

- *h*: hourly values (e.g., the integral of the global irradiance observed during one hour, which is the hourly irradiation),

- *d*: daily values (e.g., the integral of the global irradiance observed during one day, which is the daily irradiation),

- *m*: mean monthly values (e.g., the mean value of the hourly irradiation observed during one month for the hour *h*).

Notations for the irradiances and irradiations:

- $G_0^t(i,j)$ is the horizontal irradiance outside the atmosphere for the time *t* and the pixel *(i, j)*. $G_0^t(i,j) = I_0 \, \textbf{e(t)} \, sin \, \textbf{g}_S(t,i,j)$. It is expressed in W m^{-2}.

- $G_{0h}(i,j)$ is the horizontal hourly irradiation outside the atmosphere for the hour *h* and the pixel *(i, j)*. It is expressed in W h m^{-2}.

- $G_{0d}(i,j)$ is the horizontal daily irradiation outside the atmosphere for the day *d* and the pixel *(i, j)*. It is expressed in W h m^{-2}.

- $G^t(i,j)$, $B^t(i,j)$ and $D^t(i,j)$ are respectively the horizontal global, beam and diffuse irradiances at ground level for the time *t* and the pixel *(i, j)*. They are expressed in W m^{-2}.

- $G_c^t(i,j)$, $B_c^t(i,j)$ and $D_c^t(i,j)$ are respectively the horizontal global, beam and diffuse irradiances at ground level under clear sky for the time *t* and the pixel *(i, j)*. They are expressed in W m^{-2}.

- $G_h(i,j)$, $B_h(i,j)$ and $D_h(i,j)$ are respectively the horizontal global, beam and diffuse hourly irradiations at ground level for the hour *h* and the pixel *(i, j)*. They are expressed in W h m^{-2}. Similar notations hold for the daily irradiations, with a subscript *d*.

- $G_{ch}(i,j)$, $B_{ch}(i,j)$ and $D_{ch}(i,j)$ are respectively the horizontal global, beam and diffuse hourly irradiations at ground level under clear sky for the hour *h* and the pixel *(i, j)*. They are expressed in W h m^{-2}. Similar notations hold for the daily irradiations, with a subscript *d*.

2.3. Notations for describing the optical properties of the atmosphere and the ground

- $KT^t(i,j)$ is the clearness index for the time *t* and the pixel *(i, j)*. It is equal to the ratio of the global radiation at ground on a horizontal surface $G^t(i,j)$ to the horizontal radiation outside the atmosphere $G_0^t(i,j)$: $KT^t(i,j) = G^t(i,j) \, / \, G_0^t(i,j)$. The clearness index may be defined from irradiance or from hourly or daily irradiations: $KT_h(i,j)$ or $KT_d(i,j)$.

- $K_c^t(i,j)$ is the clear-sky index for the time *t* and the pixel *(i, j)*. It is equal to the ratio of the global radiation at ground on a horizontal surface $G^t(i,j)$ to the same quantity but for clear skies $G_c^t(i,j)$: $K_c^t(i,j) = G^t(i,j) \, / \, G_c^t(i,j)$. It may be defined from irradiance or from hourly or daily irradiations: $K_{ch}(i,j)$ or $K_{cd}(i,j)$.

- $T_L(AM2)$ is the Linke turbidity factor for a relative air mass *m* equal to 2.

- m is the relative optical air mass. It expresses the ratio of the optical path length of the solar beam through the atmosphere to the optical path through a standard atmosphere at sea level with the sun at the zenith.

- $\boldsymbol{d}_R(m)$ is the integral Rayleigh optical thickness.

- $L^t(i,j)$ is the radiance observed by the spaceborne for the time t and the pixel *(i, j)*. It is expressed in W m^{-2} sr^{-1}.

2.4. Notations for other properties of the site

- z is the elevation of the site above mean sea level.

- p is the pressure at site elevation and p_0 is the mean atmospheric pressure at sea level.

- $\boldsymbol{F}$ and $\boldsymbol{l}$ are respectively the latitude (positive to the Northern Hemisphere) and longitude of the site (positive eastwards).

2.5. Satellite (Meteosat) -related quantities

- S_1 is the sensor spectral response in the visible range, covering approximately the interval [0,3 µm, 1,1 µm] for Meteosat (unitless)

- I_{0met} is the total irradiance in the visible channel for the various Meteosat sensors (*i.e.* $\int_{0.3}^{1.1} I_{0l} S_1 \, d\boldsymbol{l}$), in W m^{-2}

- $\boldsymbol{r}^t(i,j)$ is the apparent albedo observed by the spaceborne sensor for the pixel *(i, j)*. It has no unit and is equal to the bidimensional reflectance, assuming the Lambertian hypothesis.
$$\boldsymbol{r}^t(i,j) = \frac{\boldsymbol{p} \, L^t(i,j)}{I_{0met} \, \boldsymbol{e}(t) \, \sin \boldsymbol{g}_S(t,i,j)} = \frac{\boldsymbol{p} \, L^t(i,j)}{I_{0met} \, \boldsymbol{e}(t) \, \cos \boldsymbol{q}_S(t,i,j)}$$

- $\boldsymbol{r}^t_{cloud}(i,j)$ is the apparent albedo observed by the spaceborne sensor over the brightest clouds for the pixel *(i, j)* (unitless) (a quantity specific to the method Heliosat)

- $\boldsymbol{r}^t_g(i,j)$ is the apparent albedo observed by the spaceborne sensor over the ground under clear skies for the pixel *(i, j)* (unitless) (a quantity specific to the method Heliosat)

- $\boldsymbol{q}_v$ is the angle between the normal to the ground and the direction of the satellite for the pixel under concern. It is the complement to 90° of the satellite altitude angle above horizon. It is called hereafter the satellite viewing angle

- $\boldsymbol{y}$ is the difference between the sun and satellite azimuth angles

- a^t, b^t and CN^t_{dark} are the calibration coefficients of the Meteosat radiometer at instant t.

2.6. Units, angles and time systems

Each quantity is expressed by the means of unit. For the same quantity, several units may be used. Care should be taken as several equations, especially those comprising constants, are valid for one unit and not another.

Note that the angles are expressed in radian or decimal degree (e.g., 30.2 °).

The True Solar Time (TST) is equivalent to the Local Apparent Time (LAT). This system of time offers the advantage of symmetry of the solar geometry about the north-south line. LMT is the Local Mean Time or clock time. The time UTC, or UT, is the Universal Time Co-ordinated; it is equivalent to the time Greenwich Meridian Time (GMT).

3.   Overview of the method Heliosat-II

3.1. Principle of the method

The principle of the method Heliosat-II, as well as most current methods, is that a difference in global radiation perceived by the sensor aboard the satellite is only due to a change in apparent albedo, which is itself due to an increase of the radiation emitted by the atmosphere towards the sensor.

A key parameter is the cloud index *n*, resulting from a comparison of what is observed by the sensor to what should be observed over that pixel if the sky were clear, which is related to the "clearness" of the atmosphere. In principle, it can be written as:

$$n^t(i,j) = [\, \boldsymbol{r}^t(i,j) - \boldsymbol{r}^t_g(i,j)\,] / [\, \boldsymbol{r}^t_{cloud} - \boldsymbol{r}^t_g(i,j))\,]$$

where

- $\boldsymbol{r}^t(i,j)$ is the reflectance, or apparent albedo, observed by the spaceborne sensor for the time *t* and the pixel *(i, j)*: $\boldsymbol{r}^t(i,j) = \dfrac{\boldsymbol{p}\,L^t(i,j)}{I_{0met}\,\boldsymbol{e}(t)\,cos\,\boldsymbol{q}_S(t,i,j)}$, where $L^t(i,j)$ is the observed radiance,

- $\boldsymbol{r}^t_{cloud}(i,j)$ is the apparent albedo over the brightest clouds,

- and $\boldsymbol{r}^t_g(i,j)$ is the apparent albedo over the ground under clear skies.

If the sky is clear, the apparent albedo $\boldsymbol{r}^t(i,j)$ is close to the apparent albedo over the ground and the cloud index *n* is close to 0 (possibly negative). If the sky is overcast, the cloud index *n* is close to 1 (possibly larger). In brief, the cloud index *n* may be considered as describing the attenuation of the atmosphere (1 minus the transmittance). Thus, the cloud index *n*, or similar quantities depending upon the methods, is a very convenient tool to exploit satellite images.

The basic principle is not always verified. Other parameters may intervene, such as multiple cloud layers and dramatic changes in the ground albedo due to the snowfall or the shadow created by a neighbouring cloud. The change in sensor outputs is not necessarily linked to a change in the optical state of the atmosphere or a change in the optical state does not necessarily translate into a change in the cloud index.

The cloud index should not be confused with the cloud cover. Given an overcast sky, the observer at ground level will report a cloud cover of 8 in okta. This cloud cover will be the same whether there is one single layer of clouds or more, while the cloud index *n* may be sensitive to the vertical profile of clouds.

The albedos used in the above equation may be constructed from a time-series of satellite images. The optical state of the clear sky is given by a model, often in the form of the global irradiation and its direct and diffuse components and the beam and diffuse transmittances.

Finally, the cloud index *n* is related to the global irradiation on an hourly (or half-hourly) basis by the means of the clearness index or the clear-sky index. From these hourly irradiations, the daily irradiation can be constructed.

3.2. Operational implementation of the method Heliosat-II

The implementation of the method is composed of four major components, shown in the following figure:

- the computation of the reflectance,

- the computation of the atmospheric reflectance,

- the computation of the cloud index,

- the computation of the irradiation.

These components are briefly described in the following figures. The equations and algorithms are detailed in the following pages.
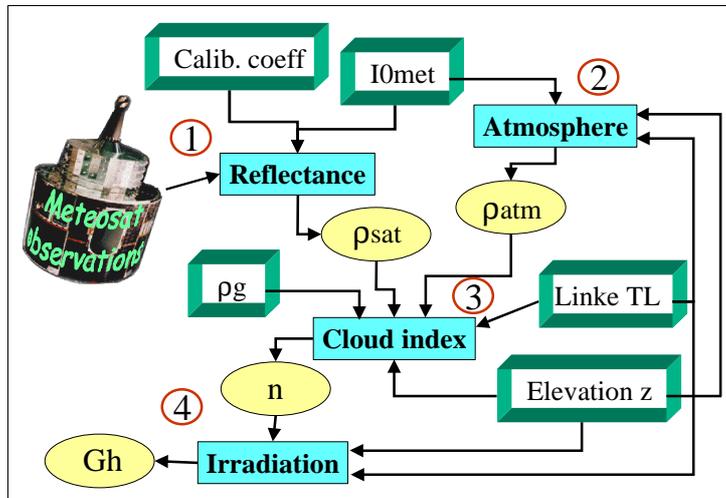
General scheme of the method Heliosat-II. It is made up of four main components, appearing in red circles.

The first component "reflectance" reads the Meteosat data and calibrates them using external information: I_{0met} and calibration coefficients. Then, the resulting radiances *Lsat* are converted into reflectances **r**sat, by the means of the procedure *calcul_albedo*. This procedure uses I_{0met}.
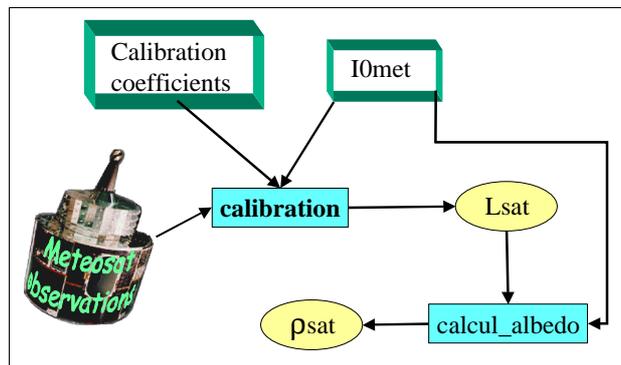
Scheme of the "reflectance" component

The second component "atmosphere" computes the radiances of the atmosphere *Latm* for the clear sky for each pixel, by the means of the procedure *calcul_Latm*, using the clear sky library and external information: the elevation *z* and the Linke turbidity factor *TL*. Then, the resulting radiances *Latm* are

converted into reflectances r_{atm}, by the means of the procedure *calcul_albedo*. This procedure uses I_{0met}.
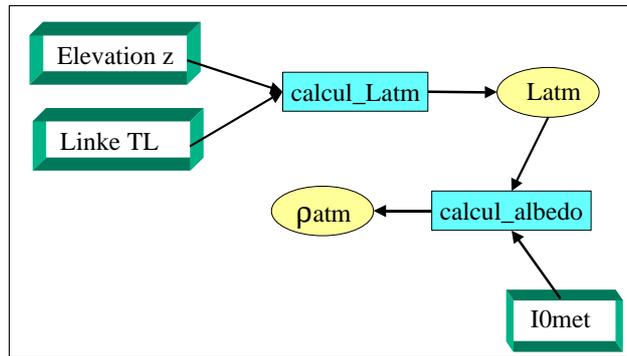
Scheme of the "atmosphere" component

The third component "cloud index" computes the cloud index *n*. The reflectances r_{sat} and r_{atm} are inputs to the procedure *calcul_rho_rhoc* that uses the elevation *z* and the Linke turbidity factor *TL* as external information. The outputs are the reflectance r^* and the cloud reflectance r_c, which are inputs to the procedure *calcul_n* to produce the cloud index *n*. This procedure calls upon external data: the ground reflectance r_g. In cases where the map of ground albedo needs to be updated, the value r^* is combined with r_g if the sky is clear to produce a new r_g value. The cloud index may be corrected of the influence of the sun glitter at the surface of the ocean if necessary.
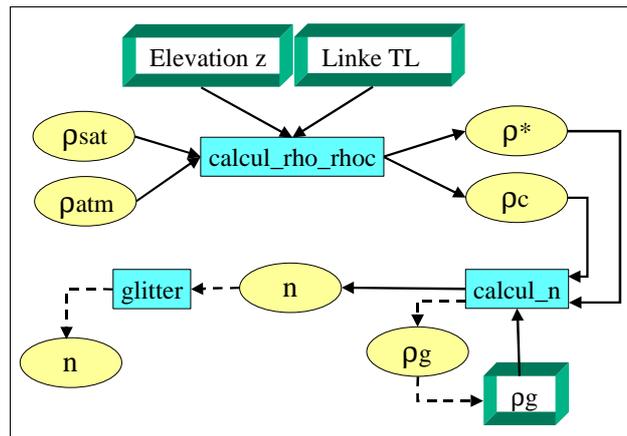
Scheme of the "cloud index" component

The fourth component "irradiation" converts the cloud index *n* into clear sky index *Kc* by the mean of the procedure *calcul_Kc*. The clear sky index is the ratio of the observed irradiation *Gh* to the clear sky irradiation *Gch* that should be observed at that site and that instant. The formula proposed by Rigollier, Wald (1999) should be corrected and that is the purpose of the procedure *correction_Kc*.

The clear sky index is an input to the procedure *calcul_Gh* that delivers the global hourly irradiation *Gh*. The procedure calls upon the clear sky library and the elevation and Linke turbidity factors as external information.
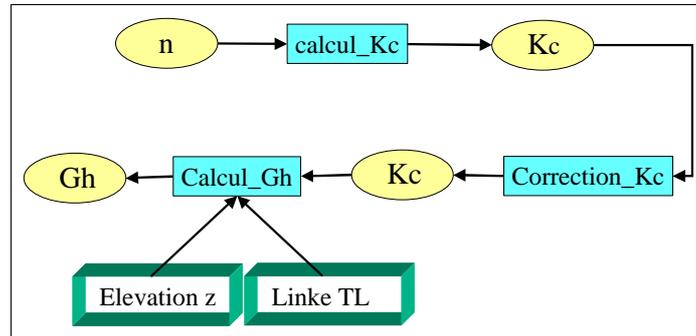
Scheme of the "irradiation" component

3.3.   About the data model

The method is independent of the choice of the data model. However, the software was written for the exploitation Meteosat images within a specific data model and this may appear in some procedures.

What should be known of this data model?

For the time sampling in the database, we use the time system of Eumetsat. The time is expressed in half-hour in UTC, noted slot, ranging from 1 to 48. The time support is still the hour, that means that the obtained irradiation value is assumed to be integrated over one hour (hourly irradiation).

Computations are all made in the True Solar Time system for more accurate results.

The irradiation output is obtained for a single pixel in this software. Many researchers average irradiation over contiguous pixels, typically 5 by 5 pixels. This leads to a lower error, as expressed in root mean square error. The bias is unchanged.

The operational implementation at Ecole des Mines is made in such a way that the database contains cloud index and not irradiation values. The cloud index, a quantity ranging between –0.2 and 1.1, is stored as a byte after an appropriate offset and multiplication. Then, computation of irradiation quantities is made on the fly, e.g. through the Web site SoDa (http://www.soda-is.com).

The original structure of the data as images is kept until the computation of the cloud index. Then, another structure is adopted that resembles to what exists for the ground stations in the World Meteorological Organization. For each pixel, is stored a time-series of all cloud indices for a full year. This change of structure appears in the software dealing with the cloud index for the computation of clearness index and irradiation. Actually, what is stored is a couple (slot, cloud index). In the HelioClim database, constructed from B2 images, only 8 slots are available per day. The day is not stored explicitly (number or date). The day is retrieved by the biunivocal relationship between the day and the address of the series of values for this day in the database, knowing that there are eight couples per day.

As the measuring stations in WMO network that have a specific identifier, we defined an identifier in our own nomenclature as follows. Scanning the Meteosat image of 416 times 416 pixels, starting from the upper left corner, we reject pixels that are outside the Earth disk as seen by Meteosat and the pixels

for which the elevation angle under which Meteosat is seen from this location, is smaller than 15° - the physical model being not accurate for such angles. The remaining pixels are labelled by their ranking order; this ranking order is the identifier.

A table is set that offers a correspondence between the identifier, the location of the pixel in lines and rows and the geographical location in latitude and longitude. Also stored are the monthly values of the Linke turbidity factor and the altitude of the pixel.

4.   Using the Web services SoDa and HelioClim

The Web services SoDa and HelioClim may be used during the implementation of the method in order to validate the correct implementations of the libraries and of the method.

4.1. Validating libraries implementation

The Soda service offers several resources that were constructed by the means of the same libraries used in Heliosat-II. These resources were carefully checked by three independent teams and through analytical calculations whenever possible.

Launching these resources permits to obtain reference data to which one may compare the outputs of the implemented software. To launch the SoDa service, launch *http://www.soda-is.com*, then click on "Run the prototype", then select the folder containing the desired resource.

4.1.1.   Position of the sun in the sky

Folder "Simulation of Radiation under Clear Skies", resource "position of the sun in the sky".

This resource provides, for a given day and a given latitude:

- declination,

- time for sun set and sunrise as well as day length,

- elevation and azimuth of the sun at any instant.

One may validate the correct implementation and use of the library *solar_geometry.c*. Angles are in decimal degree, time is in decimal hour. Time is the True Solar Time (that is why there is no input in longitude).

4.2.1.   Correct reading of the Linke turbidity factor database

Folder "Climatological Data and Derived Quantities", sub-folder "Climatological Data", resource "Monthly values of Linke turbidity factor".

One may get the Linke turbidity factor (TL) for all months for any site. This permits to check the correct reading of the TL values in the files *tl.zip* collected from the *heliosat* Web site.

4.3.1.   Simulating the clear sky values

Folder "Simulation of Radiation under Clear Skies", resource "Hourly irradiation for one day".

For given day, latitude, longitude, elevation and Linke turbidity factor, this resource predicts the daily profile and sum of hourly irradiation for clear skies using the modified ESRA clear sky used in Heliosat-II. Outputs are the global irradiation as well as its direct and diffuse components for the day and each hour. Time is in decimal hour and is the True Solar Time.

Using this resource permits to validate the correct implementation and use of the library *csmodels_lib.c*.

4.2. Validating the whole method

The Soda service may also be used in order to compare the outputs of the proposed implementation with the assessments derived from the database HelioClim that can be accessed through the SoDa service "long-term time-series of irradiation / Daily Irradiation / Meteosat-derived data – Europe / Africa ".

4.3. Checking data quality

The HelioClim server (http://www.helioclim.net) offers a service that permits to check the quality of irradiation data. This may be useful before any comparison between outputs of the method Heliosat-II and irradiation data acquired by pyranometers. This service is fully described in Geiger *et al.* (2003). Data are pasted in a box in a form appearing on the browser. An indicator is returned with each data, stating if problems were detected or nor, and if yes, which type of problem.

5. List of libraries

Name	Object
clearsky_model5_lib.c	Modelling the irradiance and irradiation under clear-skies. Uses the following library
csmodels_lib.c	Modelling the irradiance and irradiation under clear-skies. Basic functions
glitter_lib.c	Correction of glitter effects
helio.h	Not a library. Contains a number of global variables and functions
map_cloud.c	**Is not a library**. Is a software including several libraries. Demonstrates how the various components are assembled for obtaining the cloud index
map_lib.c	Calibration, computation of the reflectance, computation of the clear-sky index, hourly irradiation, clearness index, and daily irradiation
map_rhog.c	**Is not a library**. Is a software including several libraries. Demonstrates how the ground albedo can be obtained
map_rhog_ref.c	**Is not a library**. Is a software including several libraries. Demonstrates how the reference ground albedo can be obtained
meteosatlib.c	Geometry of the satellite (elevation, azimuth) with respect to the pixel, and conversion latitude – longitude into satellite co-ordinates row – columns
solar_geometry.c	Solar geometry, extraterrestrial irradiation, time system
spatio_time_lib.c	Contains functions for getting information about sun geometry, Linke turbidity factor, elevation ... for a given pixel. Includes also functions about leap year and julian days and spatial interpolation

5.1. Formats used in C

char   character, 1 byte

u_char   unsigned character, 1 byte

short_int   integer, 2 bytes

int   integer, 4 bytes

float   real, 4 bytes

double precision   real, 8 bytes

All computations should be made in double precision, if real numbers are involved.

5.2. Library "solar_geometry.c"

The library "solar_geometry.c" is made of several procedures for computing the solar geometry and extraterrestrial irradiation. It comprises the following items:

- geometry of the solar beam,

- sunrise, sunset and day length,

- changing the time system,

- position of the sun in the sky,

- extraterrestrial irradiation,

- integrated procedures providing the above parameters for a given day, or on monthly or yearly averages.

5.3. Library "meteosatlib.c"

The library "meteosatlib.c" is made of several useful functions for computing the geometry of the satellite (elevation, azimuth) with respect to the pixel, and to convert latitude – longitude into satellite co-ordinates row – columns.

There are two Meteosat products treated in this library:

1. a high resolution image (noted HR) with 2500 lines and 2500 pixels per line oriented NW (lig 1, col 1) to SE (lig 2500, col 2500). The pixel size is 5 km at nadir. When such coordinates in lines and columns are used, they always refer to the image correctly oriented NW-SE. Note that the acquired image is actually inverse, taken from SE to NW, so that the first pixel acquired within a time frame is the south-easternmost pixel on the image (2500, 2500).

2. a B2 image (noted B2) with 416 lines and 416 pixels per line, subsampled from the high resolution as follows: starting from the first pixel acquired (2500, 2500) are taken each pixel every 6 lines and every 6 columns. These selected pixels are noted HRb2 in the high resolution product, and B2 in the B2 product. Thus, a pixel B2 represents a pack of 6x6 HR pixels whose south-easternmost one substitutes the other ones. Note that 6 cannot divide 2500, so that the B2 product ignores the last 4 lines and columns in the acquired direction. The first HRb2 pixel is positioned (10,10) on the high resolution image, while the last one is (2500, 2500) using a correctly oriented HR image.

It comprises the following items:

- converting latitude – longitude to HR co-ordinates and reverse,

- converting latitude – longitude to B2 co-ordinates,

- relationship between HR pixels, HRb2 pixels and B2 pixels in their respective frames,

- elevation angle of the satellite seen from the ground and azimuth (and consequently the satellite viewing angle).

6. Modelling the global, direct and diffuse irradiations under clear-skies

Let note the latitude of the site (positive to the Northern Hemisphere), $\boldsymbol{F}$, its longitude (positive eastwards), $\boldsymbol{l}$, its elevation above mean sea level, z, the declination of the sun for the day under concern, $\boldsymbol{d}$, and the solar hour angle for the instant t, $\boldsymbol{w}$. The sun elevation above horizon, $\boldsymbol{g}_s^{true}$, corrected for refraction is given in radians by:

$$\boldsymbol{g}_s^{true} = \boldsymbol{g}_s + \boldsymbol{Dg}_{refr}$$

$$sin\boldsymbol{g}_S = sin\boldsymbol{F} sin\boldsymbol{d} + cos\boldsymbol{F} cos\boldsymbol{d} \ cos\boldsymbol{w}$$

$$\boldsymbol{Dg}_{refr} = 0.061359 \frac{0.1594 + 1.123 \ \boldsymbol{g}_S + 0.065656 \ \boldsymbol{g}_S^2}{1 + 28.9344 \ \boldsymbol{g}_S + 277.3971 \ \boldsymbol{g}_S^2}$$

The modelling of the irradiation for clear skies originates from the clear-sky model of the European Solar Radiation Atlas (ESRA 2000; Rigollier *et al.* 2000) with corrections for the site elevation proposed by Remund, Page (2002).

The relative optical air mass *m* expresses the ratio of the optical path length of the solar beam through the atmosphere to the optical path through a standard atmosphere at sea level with the sun at the zenith. As the solar altitude decreases, the relative optical path length increases. The relative optical path length also decreases with increasing site height. A correction procedure is applied, obtained as the ratio of mean atmospheric pressure, *p*, at the site elevation, to mean atmospheric pressure at sea level, p_0. This correction is particularly important in mountainous areas. The relative optical air mass at sea level has no unit and is given by Kasten, Young (1989):

$$m(\boldsymbol{g}_s^{true}) = 1 \ / \ [\ sin \ \boldsymbol{g}_s^{true} + 0.50572 \ ((180/\boldsymbol{p})\boldsymbol{g}_s^{true} + 6.07995)^{-1.6364}]$$

The Rayleigh optical thickness, $\boldsymbol{d}_R$, is the optical thickness of a pure Rayleigh scattering atmosphere, per unit of air mass, along a specified path length. As the solar radiation is not monochromatic, the Rayleigh optical thickness depends on the precise optical path and hence on relative optical air mass, *m*. The parameterisation used is based on Kasten (1996) and was modified by Remund, Page (2002) to correct the behaviour of the original model with terrain altitude.

The height correction is given by

$$p/p_0 = exp(-z/z_h)$$

where z_h is the scale height of the Rayleigh atmosphere near the Earth surface, equal to 8434.5 meters.

Let $corr\_\boldsymbol{d}_R(p/p_0)$ be the correction of the integral Rayleigh optical thickness due to the elevation of the site. Remund, Page determined this function for two values of (p/p_0):

$$corr\_\boldsymbol{d}_R \ (0.75) = 1.248174 - 0.011997 \ m(\boldsymbol{g}_s^{true}) + 0.00037 \ m^2(\boldsymbol{g}_s^{true})$$

$$corr\_\boldsymbol{d}_R \ (0.50) = 1.68219 - 0.03059 \ m(\boldsymbol{g}_s^{true}) + 0.00089 \ m^2(\boldsymbol{g}_s^{true})$$

Given that $corr\_\boldsymbol{d}_R(1)=1$ and assuming that $corr\_\boldsymbol{d}_R(p/p_0) = corr\_\boldsymbol{d}_R(0.5)$ for $(p/p_0)>0.5$, $corr\_\boldsymbol{d}_R(p/p_0)$ can be determined for any (p/p_0) by piecewise linear interpolation. The integral Rayleigh optical thickness is thus given by:

if m $\pounds$ 20, ($\boldsymbol{g}_S$ ^{3} 1.9°)

$1/\boldsymbol{d}_R(m) = corr\_\boldsymbol{d}_R \ (p/p_0) \ [6.625928 + 1.92969m \ -0.170073m^2 \ +0.011517m^3 \ -0.000285m^4 \ ]$

if m > 20, ($\boldsymbol{g}_S$ < 1.9°), $1/\boldsymbol{d}_R(m) = 10.4 + 0.718 \ m \ (p/p_0)$

6.1. The beam component

The beam irradiation for a period ranging from solar hour angles w_1 to w_2, is given by:

$$B_c(w_1, w_2) = I_0 \, e \, \frac{Dl}{2p} T_{rb}(T_L(AM2)) \int_{w_2}^{w_1} F_b(g_s, T_L(AM2)) \, dw$$

where

- e is the correction of the variation of sun-earth distance for the day under concern. $I_0 \, e$ is the extraterrestrial irradiance for the current day observed on a surface normal to the solar beam.

- Dl is the average length of the day (*i.e.*, 24 hours). The unit of B_c is Wh m^{-2} if Dl is expressed in hours, or J m^{-2} if Dl is in seconds.

- w_1 to w_2 are related to two instants t_1 and t_2.

$T_{rb}(T_L(AM2))$ is a transmission function for beam radiation at zenith ($g_s = p/2$), function of the Linke turbidity factor, $T_L(AM2)$, and F_b is a beam angular function. B_c is set to 0 if the equation leads to a negative value. $T_{rb}(T_L(AM2))$ and $F_b(g_s, T_L(AM2))$ are given by:

$$T_{rb}(T_L(AM2)) = exp[-0.8662 \, T_L(AM2) \, (p/p_0) \, d_R(p/p_0)]$$

$$F_b(g_s, T_L(AM2)) = C_0 + C_1 sin(g_s) + C_2 sin^2(g_s)$$

The values of the coefficients C_0, C_1 and C_2 are polynomials and are given for three ranges of the solar altitude angle at noon, g_s^{noon}: below 15°, between 15° and 30°, and over 30°:

$$C_0 = L_{00} + L_{01} \, T_L(AM2) \, (p/p_0) + L_{02} \, [T_L(AM2) \, (p/p_0)]^2$$

$$C_1 = L_{10} + L_{11} \, T_L(AM2) \, (p/p_0) + L_{12} \, [T_L(AM2) \, (p/p_0)]^2$$

$$C_2 = L_{20} + L_{21} \, T_L(AM2) \, (p/p_0) + L_{22} \, [T_L(AM2) \, (p/p_0)]^2 + L_{23} \, [T_L(AM2) \, (p/p_0)]^3$$

with the L_{ij} coefficients listed in Table 1. These coefficients, as well as the coefficients A_i, B_i, C_i and D_i (see further) are unitless.

C_0	L_{00}	L_{01}	L_{02}	
$g_s^{noon} > 30^0$	$-1.7349.10^{-2}$	$-5.8985.10^{-3}$	$6.8868.10^{-4}$	
$15^0 < g_s^{noon} £ 30^0$	$-8.2193.10^{-3}$	$4.5643.10^{-4}$	$6.7916.10^{-5}$	
$g_s^{noon} £ 15^0$	$-1.1656.10^{-3}$	$1.8408.10^{-4}$	$-4.8754.10^{-7}$	

C_1	L_{10}	L_{11}	L_{12}	
$g_s^{noon} > 30^0$	1.0258	$-1.2196.10^{-1}$	$1.9229.10^{-3}$	
$15^0 < g_s^{noon} £ 30^0$	$8.9233.10^{-1}$	$-1.9991.10^{-1}$	$9.9741.10^{-3}$	
$g_s^{noon} £ 15^0$	$7.4095.10^{-1}$	$-2.2427.10^{-1}$	$1.5314.10^{-2}$	

C_2	L_{20}	L_{21}	L_{22}	L_{23}
$g_s^{noon} > 30^0$	$-7.2178.10^{-3}$	$1.3086.10^{-1}$	$-2.8405.10^{-3}$	0
$15^0 < g_s^{noon} £ 30^0$	$2.5428.10^{-1}$	$2.6140.10^{-1}$	$-1.7020.10^{-2}$	0
$g_s^{noon} £ 15^0$	$3.4959.10^{-1}$	$7.2313.10^{-1}$	$-1.2305.10^{-1}$	$5.9194.10^{-3}$

Table 1 *Coefficients L_{ij} for the computation of the C_i coefficients.*

$F_b(g_s, T_L(AM2))$ can be rewritten as a function of w, F, d, $T_L(AM2)$:

$$F_b(w, F, d, T_L(AM2)) = B_0 + B_1 \, cosw + B_2 \, cos(2w)$$

since

$$sing_S = sinF \, sind + cosF \, cosd \, cosw$$

It comes

$$B_c(w_1, w_2) = I_0 \, e \, \frac{Dl}{2p} T_{rb}(T_L(AM2)) \, [B_0 w + B_1 \, sin(w) + B_2 \, sin(2w)] \, _{w_1}^{w_2}$$

with the coefficients B_0, B_1 and B_2 given by:

$$B_0 = C_0 + C_1 \, sin(F) \, sin(d) + C_2 \, sin(F)^2 \, sin(d)^2 + 0.5 \, cos(F)^2 \, cos(d)^2$$

$$B_1 = C_1 \, cos(F) \, cos(d) + 2 \, C_2 \, sin(F) \, sin(d) \, cos(F) \, cos(d)$$

$$B_2 = 0.25 \, C_2 \, cos(F)^2 \, cos(d)^2$$

The daily integral is achieved by setting w_1 equal to the sunrise hour angle, w_{SR}, and w_2 to the sunset hour angle, w_{SS}, *i.e.*:

$$B_{cd} = B_c(w_{SR}, w_{SS})$$

6.2. The diffuse component

The diffuse horizontal irradiation, $D_c(w_1, w_2)$, over any period defined by w_1 and w_2, is given by:

$$D_c(w_1, w_2) = I_0 \, e \, \frac{Dl}{2p} T_{rd}(T_L*(AM2)) \, [D_0 w + D_1 \, sin(w) + D_2 \, sin(2w)] \, _{w_1}^{w_2}$$

where $T_L*(AM2) = p/p_0 \, T_L(AM2)$.

The transmission function at zenith, T_{rd}, is given by

$$T_{rd}(T_L*(AM2)) = -1.5843 \, 10^{-2} + 3.0543 \, 10^{-2} \, T_L*(AM2) + 3.797 \, 10^{-4} \, T_L*(AM2)^2$$

The coefficients D_0, D_1 and D_2 are given by:

$$D_0 = A_0 + A_1 \, sin(F) \, sin(d) + A_2 \, sin(F)^2 \, sin(d)^2 + 0.5 \, cos(F)^2 \, cos(d)^2$$

$$D_1 = A_1 \, cos(F) \, cos(d) + 2 \, A_2 \, sin(F) \, sin(d) \, cos(F) \, cos(d)$$

$$D_2 = 0.25 \, A_2 \, cos(F)^2 \, cos(d)^2$$

The coefficients A_0, A_1, and A_2, are given by:

$$A_0 = 2.64631 \, 10^{-1} - 6.1581 \, 10^{-2} \, T_L*(AM2) + 3.1408 \, 10^{-3} \, T_L*(AM2)^2$$

$$A_1 = 2.0402 + 1.89451 \, 10^{-2} \, T_L*(AM2) - 1.1161 \, 10^{-2} \, T_L*(AM2)^2$$

$$A_2 = -1.3025 + 3.9231 \, 10^{-2} \, T_L*(AM2) + 8.5079 \, 10^{-3} \, T_L*(AM2)^2$$

with a condition on A_0:

$$if \, (A_0 \, T_{rd}) < 2 \, 10^{-3} \, then \, A_0 = 2 \, 10^{-3} / T_{rd}$$

This condition is required because A_0 yields negative values for $T_L(AM2)>6$. It was therefore decided to impose this limiting condition to achieve acceptable values at sunrise and sunset.

The daily integral is achieved by setting w_1 equal to the sunrise hour angle, w_{SR}, and w_2 to the sunset hour angle, w_{SS}, *i.e.*

$$D_{cd} = D_c(w_{SR}, w_{SS})$$

6.3. The global irradiation

The global irradiation under clear sky, G_c, is obtained as the sum of the beam and diffuse horizontal irradiations under clear sky between two instants t_1 and t_2.

$$G_c(w_1, w_2) = B_c(w_1, w_2) + D_c(w_1, w_2)$$

The parameters w_1 and w_2 are respectively set to w_{SR} and w_{SS} for the computation of the daily global irradiation:

$$G_c(w_{SR}, w_{SS}) = B_c(w_{SR}, w_{SS}) + D_c(w_{SR}, w_{SS}) \ \hat{U} \ G_{cd} = B_{cd} + D_{cd}$$

One may define the global transmittance of the atmosphere for the incident radiation, $T(q_S)$, as the sum of the beam and diffuse transmittances:

$$T(q_S) = Tr_B(q_S) + Tr_D(q_S)$$

6.4. The library csmodels_lib.c

This library comprises a set of procedures and functions that reproduce the equations of the clear sky model. This model is named *model5* in this library. Other functions are available, especially the computation of the Rayleigh optical depth and the Linke turbidity factor, depending on various models.

Several routines compute the following quantities, separately or in a aggregated form:

- clear sky beam transmittance for beam radiation, Trb,

- clear sky beam angular function for beam irradiation, Fb,

- clear sky transmittance at zenith for diffuse radiation, Trd, and diffuse angular function, Fd,

- clear sky direct irradiance, Bc (in W/m2), beam and horizontal, as well as irradiation (in Wh/m2),

- clear sky diffuse irradiance, Dc (in W/m2), and irradiation (in Wh/m2),

- clear sky global irradiance, Gc (in W/m2), and irradiation (in Wh/m2),

- clear sky daily global irradiation Gcd (in Wh/m2), as well direct horizontal Bcd and diffuse Dcd,

- clear sky 24-hourly global irradiation Gch (in Wh/m2), as well direct horizontal Bch and diffuse Dch,

- same but averaged over a month,

- same but averaged over a year.

7. The ground albedo

Given the radiance $L^t(i,j)$ observed by a Meteosat sensor at instant t and for the pixel (i,j), and I_{0met} the total irradiance in the visible channel for this sensor, the reflectance, or apparent albedo, is:

$$r^t(i,j) = \frac{p\, L^t(i,j)}{I_{0met}\, e(t)\, cosq_S(t,i,j)}$$

where q_S is the sun zenithal angle.

7.1. The reflectance of the ground

The reflectance observed by the sensor r^t_{sat} under clear skies is a function of the reflectance of the ground, r^t_g, the sun zenithal angle, q_S, the satellite viewing angle, q_v, (i.e., the complement to 90° of the satellite altitude angle) and the difference, y, of the sun and satellite azimuth angles. At the first order, given the large size of the pixel, the multiple reflection and scattering effects are negligible. Assuming a Lambertian ground, the reflectance observed by the sensor is (Tanré *et al.* 1990):

$$r^t_{sat}(i,j) = r^t_{atm}(q_S,\ q_v, y) + r^t_g(i,j)\, T^t(q_S)\, T^t(q_v)$$

where $r^t_{atm}(q_S,\ q_v, y)$ is the intrinsic reflectance of the atmosphere, caused by the scattering of the incident and upward radiation towards the sensor. It is also called the path reflectance. The parameters $T^t(q_S)$ and $T^t(q_v)$ are the global transmittances of the atmosphere for the incident and upward radiation. The principle of reciprocity implies that the same formulation applies to both transmittances.

Numerous works show that the ground is not exactly of Lambertian nature. Vermote *et al.* (1994) propose several bi-directional models to consider these effects in the simulation of $r^t_{sat}(i,j)$. From an operational point of view, the method Heliosat-II cannot consider these effects by lack of information. In particular, it would imply the knowledge of the landuse for each pixel of the field of view of the satellite Meteosat and of the associated model.

The influence of the sun zenithal angle q_S is important as well as that of the Linke turbidity factor, which affects the transmittance. The air mass increases with q_S, causing an increase of the intrinsic reflectance of the atmosphere r^t_{atm}. The transmittance decreases as the turbidity increases, or similarly as the visibility decreases. The difference, y, of the sun and satellite azimuth angles impacts on the reflectance observed by the sensor, though it is less important than the sun zenithal angle.

The present approach is based upon the modelling of the intrinsic reflectance of the atmosphere, also called the path reflectance, and the atmospheric transmittance. Each term, r^t_{atm} and $T^t(q_S)$ or $T^t(q_V)$ is modelled, resulting into the explicit formulation of r^t_{sat} as a function of q_S, q_V, y and r^t_g. Inversely, this permits to compute r^t_g and r^t_{cloud}.

7.2. The atmospheric path reflectance r_{atm}

Assuming that the scattering by the atmosphere is isotropic, it is conceivable that the path radiance L_{atm} reaching the sensor is proportional to the path radiance reaching the ground. This path radiance can be expressed using the expression of the diffuse irradiance under clear sky at ground level, D_c:

$$L_{atm} = (D_c / p)\, (I_{0met} / I_0)\, (<cosq_V> / cosq_V)^{0,8}$$

The ratio (I_{0met} / I_0) normalises the extraterrestrial irradiance to the Meteosat sensor case. Following Beyer *et al.* (1996), the ratio $(<cosq_V> / cosq_V)^{0,8}$ empirically corrects for the satellite viewing angle without bias $(<cosq_V> = 0.5)$.

Various tests show that the approach is satisfactory, provided it is restricted to solar zenithal angles and satellite viewing angles less than 75°, as was the case with the method Heliosat-I (Diabaté 1989;

Bauer 1996). It follows that the method Heliosat-II will be unable in principle to accurately estimate the irradiation north of the latitude 65° N, and south of the latitude 65° S.

Knowing the Linke turbidity factor and the site elevation, the path radiance L_{atm} is computed (*procedure calcul_Latm*) and (*procedure calcul_albedo*):

$$\boldsymbol{r}^t_{atm}(\boldsymbol{q}_S, \boldsymbol{q}_v, \boldsymbol{y}) = \frac{\boldsymbol{p}\, L^t_{atm}(i,j)}{I_{0met}\, \boldsymbol{e}\, cos\boldsymbol{q}_S}$$

Finally, we get a quantity $\boldsymbol{r}^{*t}(i,j)$ that is a ground reflectance or ground albedo if the sky were clear at the instant t (*procedure calcul-rho_rhoc*):

$$\boldsymbol{r}^{*t}(i,j) = [\, \boldsymbol{r}^t_{sat}(i,j) - \boldsymbol{r}_{atm}(\boldsymbol{q}_S, \boldsymbol{q}_v, \boldsymbol{y})]\, /\, T(\boldsymbol{q}_S)\, T(\boldsymbol{q}_v)$$

where $T(\boldsymbol{q}_S)$ and $T(\boldsymbol{q}_v)$ are assessed by the means of the clear sky model (*procedure calcul-rho_rhoc*).

Library: clearsky_model5_lib.c (procedures calcul_Latm, calcul_albedo and calcul-rho_rhoc)

7.3. Constructing a map of ground albedo

The computation of the cloud index requests the knowledge of the ground albedo $\boldsymbol{r}_g(i,j)$ at each pixel. This map of ground albedo should be constructed before routinely processing the Meteosat data. In a paradoxical way, it is constructed using the Meteosat data, as done in the original method Heliosat (Cano *et al.* 1986). The principle is the following. Given a time series of reflectances observed by satellite for each pixel, it is assumed that there exist instants for which the sky was clear. I is further assumed that for clear skies, the observed reflectance is less than for cloudy skies, and thus the ground albedo may be computed from the minima of the time series.

The analysis of several years of images from Meteosat shows that it happens that some pixels exhibit very low radiances, similar to those observed during the night, while the sun is well above the horizon. A constraint is imposed on radiances to avoid such cases; they should be greater than 3 percent of the maximal radiance that can be observed by the sensor:

$$L^t(i,j)\, \text{³}\, 0,03\, \frac{I_{0met}(t)}{\boldsymbol{p}} + b(t)$$

where $b(t)$ is the calibration coefficient, and more exactly the radiance measured when viewing darkness.

A time series of reflectances $\boldsymbol{r}^{*t}(i,j)$ is obtained from a time series of Meteosat observations (*library clearsky_model5_lib.c, procedure calcul_rho_rhoc*). To eliminate artefacts in assessing the ground albedo, the time series is restricted to the instants for which the sun zenithal angle $\boldsymbol{q}_S$ is less than the maximum of 50° and (2 $\boldsymbol{q}_S^{noon}$ / 3), where $\boldsymbol{q}_S^{noon}$ is the angle observed at noon, remembering that $\boldsymbol{q}_S$ is less than 75° in any case (*see software map_rhog.c*). Once the time series established, the first and second minima are searched. The absolute minimum is subject to undetected defects in the original image and is more variable than the second minimum. This second minimum of the series of retained reflectances is the ground albedo $\boldsymbol{r}_g(i,j)$ for this period.

The time series comprises only instants for which

$$\boldsymbol{g}_S > min[\, max(\boldsymbol{g}_S^{min}, (2\, \boldsymbol{g}_S^{noon}\, /\, 3)),\, 40°]$$

where $\boldsymbol{g}_S^{noon}$ is the elevation angle observed at noon and $\boldsymbol{g}_S^{min}$ is the minimum elevation angle. Below this value, the method Heliosat is not valid. The value is set from experience to 15° ($\boldsymbol{q}_S \leq 75°$), as in Cano *et al.* All elevation angles in the above equation and others are greater than or equal to $\boldsymbol{g}_S^{min}$.

The period of the time-series should be the shortest as possible in order to take into account the rapid variations of the ground albedo, if any. Compared to the method Heliosat-I, wherein it is preferable to

have one estimate of the ground albedo per slot, the accurate correction of the effects of the sun and satellite angles permits to merge all the slots into the time-series. Thus, the period may be shortened. There is only one map of ground albedo and this map may be used for all slots.

7.4. Constructing a background albedo map

There is no certainty that the time series exhibits at least two clear sky instants and there is no guarantee that the second minimum detected is that of the ground and not a more reflective cloud. There are geographical areas that are covered by clouds for most of the year.

This possibility to have only one albedo map for a period permits to create a background map that allows overcoming the case where at a pixel, no cloudless instant is observed   (*see software map_rhog_ref.c*). Prior being declared a ground albedo, the second minimum is compared to the background value. It cannot be less to half this value and cannot be greater than twice this value. If it is the case, it is set to one of these limits. The result is the ground albedo. Denoting the background value r_{ref}, the ground albedo r_g is given by:

$$r_g = max[\ min(r_g,\ 2r_{ref}),\ r_{ref}\ /\ 2]$$

In the specific case of the construction of our database HelioClim, the background map was created by processing all images available for the months of January and December for the years 1985 to 1997. These months were selected as offering less questionable pixels for the whole field of view of the Meteosat satellite. For each pixel, the time-series of reflectances $r*^t(i,j)$ was processed as mentioned above. The background value r_{ref} is equal to the second minimum. If less than 0.05 and if the pixel is over the land, r_{ref} is set to 0.05. This background map was carefully screened by two operators to detect possible defects, using vegetation atlases and other geographical information. It is possible to construct several background maps in cases where changes in albedo are very large.

7.5. Operating in real time with a rolling map of ground albedo

In an operational mode, especially when real time is at stake, a moving period may be adopted. That means that the map of ground albedo is updated. If at an instant *t*, the cloud pixel is low (clear sky), then a new ground albedo is computed as, e.g., a linear combination of $r*^t(i,j)$ and r_g:

$$new\ r_g = [a\ r_g + b\ r*\ ]/(a+b)$$

where *a* and *b* are selected in agreement with the duration of the period. E.g., if a period of 7 days is selected with *n* slots per day, one may select *a=7n-1* and *b=1*. In that way, a complete change in albedo is performed in 7 days if all slots are clear. If *a=6* and *b=1*, only 7 clear slots are requested during the period to change the albedo.

In that case, it is important to store albedoes as real numbers and not integers.

8.   The computation of the cloud albedo

The albedo of the clouds r_{cloud} has been defined by Cano (1982) as the typical value for the brightest clouds. The histogram of cloud albedoes is flat and it is very difficult to characterise this parameter r_{cloud} by a statistical quantity, such as a mode or a percentile. Costanzo (1994) or Hammer *et al.* (1997a, b) compute the mean value of the brightest albedoes observed in a time-series of images. The results may depend upon the length of the time-series and of the selected threshold. It should be added that some sites exhibit clear skies during several months (e.g. the Mediterranean basin), making it difficult to find very bright clouds.

The above-mentioned difficulties disappear if one is using calibrated radiances. In this case, we may adopt an actual albedo of the brightest clouds. Rigollier (2000) refers to the maximum value given by Grüter *et al.* (1986), that is 0.9. According to the experience of L. Wald, who set up several implementations of the Heliosat-I method for various cases, as well as to the works of Möser, Raschke (1983), Grüter *et al.* (1986), Moussu *et al.* (1989), Stuhlmann *et al.* (1990), Raschke *et al.* (1991) and Wald (1998), this parameter is not a maximum value and should not be taken too high. The effective cloud albedo depends upon the sun zenithal angle. We follow the model proposed by Taylor, Stowe (1984a):

$$r^{t}_{eff}(i,j) = 0.78 - 0.13 \ [1 - exp(-4 \cos(q_S)^5]$$

However, the parameter r_{cloud} is to be compared to the quantities $r*^{t}(i,j)$ that derive from the observed radiances to compute the cloud index n. For $r*^{t}(i,j) = r^{t}_{cloud}(i,j)$, the cloud index n should be equal to unity. It follows that the same equation should apply to the effective cloud albedo, leading to the apparent cloud albedo $r^{t}_{cloud}(i,j)$:

$$r^{t}_{cloud}(i,j) = [\ r^{t}_{eff}(i,j) - r^{t}_{atm}(q_S, q_v, y)] \ / \ T(q_S) \ T(q_v)$$

Two constraints are added, gained from experience:

$$r^{t}_{cloud}(i,j) > 0.2, \ otherwise \ r^{t}_{cloud}(i,j) = 0.2$$

$$and \ r^{t}_{cloud}(i,j) < 2.24 \ r_{eff}(i,j), \ otherwise \ r^{t}_{cloud}(i,j) = 2.24 \ r^{t}_{eff}(i,j)$$

The value 2.24 is the largest anisotropy factor observed by Taylor, Stowe (1984b) for the present geometrical configuration sun-pixel-sensor and thick water cloud.

Library: clearsky_model5_lib.c (procedure calcul_rho_rhoc)

9. The cloud index and its relationship with the global hourly irradiation

9.1. The cloud index

The cloud index n is defined as:

$$n^t(i,j) = [\mathbf{r}^{*t}(i,j) - \mathbf{r}^t_g(i,j)] / [\mathbf{r}^t_{cloud} - \mathbf{r}^t_g(i,j))]$$

with the following constraints:

$$\text{if } \mathbf{r}^{*t}(i,j) < 0.01 \quad n^t(i,j) = 0.0$$

$$\text{if } -0.01 < [\mathbf{r}^{*t}(i,j) - \mathbf{r}^t_g(i,j)] < 0.01 \quad n^t(i,j) = 0.0$$

$$\text{if } [\mathbf{r}^t_{cloud} - \mathbf{r}^t_g(i,j))] \, £ \, 0.1 \quad n^t(i,j) = 1.2 \text{ (arbitrary large value)}$$

The cloud index is limited to –0.5 and 1.5.

Library: map_lib.c (procedures calcul_n)

9.2. The relationship between the cloud index and the global hourly irradiation

The clear-sky index K_{ch} is equal to the ratio of the hourly global irradiation at ground on a horizontal surface G_h to the same quantity but for clear skies G_{ch}:

$$K_{ch} = G_h / G_{ch} \, \hat{U} \, G_h = K_{ch} \, G_{ch}$$

A relationship between the cloud index and the clear-sky index K_{ch} was proposed by Rigollier, Wald (1999) as follows:

$$n^t < -0.2 \quad K_{ch} = 1.2$$

$$-0.2 < n^t < 0.8 \quad K_{ch} = 1 - n$$

$$0.8 < n^t < 1.1 \quad K_{ch} = 2.0667 - 3.6667\, n^t + 1.6667(n^t)^2$$

$$n^t > 1.1 \quad K_{ch} = 0.05$$
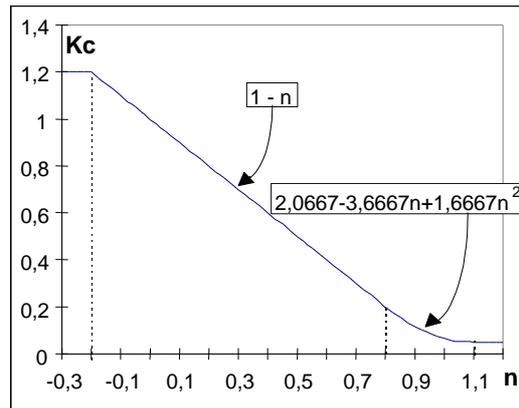
Relationship between the clear-sky index K_{ch} and the cloud index n

Detailed analyses of the discrepancies between ground measurements and Heliosat-II estimates revealed a bias that is a function of the true solar time. The exact reasons are unknown. They are believed to be a consequence of the approximate modelling of the influence of the solar zenithal angle in the joint assessment of the ground albedo, cloud albedo and instantaneous albedo.

The influence is not large at all and amounts to approximately 1-2 % in relative value. However, correcting for bias is very important in climate studies. An additional correction is brought to the clear-sky index, K_{ch}:

$$new\ K_{ch} = K_{ch} - 0.01(8\ TST - 104)$$

where *TST* is the true solar time, and

$$new\ K_{ch} = max(new\ K_{ch},\ 0.05)$$

$$new\ K_{ch} = min(new\ K_{ch},\ 1.2)$$

Obtaining the clear sky index leads to the hourly global irradiation

$$G_h = K_{ch}\ G_{ch}$$

Library: map_lib.c (procedures calcul_Kc, correction_Kc and calcul_Gh)

10.   The computation of the daily irradiation and subsequent quantities

The computation of the daily irradiation $G_d(i,j)$ is based upon the N assessments of the hourly irradiation $G_h(i,j)$ made during the day. The equations are the followings:

$$G_d(i,j) = K_{cd}(i,j)\, G_{cd}(i,j) = G_{cd}(i,j)\ \sum_{h=1}^{N} w_h\, K_{ch}(i,j)$$

where $w_h = \dfrac{G_{ch}(i,j)}{\displaystyle\sum_{h=1}^{N} G_{ch}(i,j)}$

It comes

$$G_d(i,j) = G_{cd}(i,j)\ \frac{\displaystyle\sum_{h=1}^{N} G_h(i,j)}{\displaystyle\sum_{h=1}^{N} G_{ch}(i,j)}$$

The estimate is said valid if at least N hourly irradiations are used in the computation. For each hourly irradiation, the mean solar elevation should be greater than 15°. To account for seasonal variation, N is set equal to a function of the sun zenithal angle observed at noon, q_s^{noon}.

if $q_s^{noon} < 55°$, $N = 2$; otherwise $N = 3$ for the B2 data (data available every 3 hours)

if $q_s^{noon} < 55°$, $N = 5$; otherwise $N = 8$ when hourly values are available

Other quantities are subsequently computed: the cumulative of the daily irradiation during 5 days or 10 days and the monthly mean of the daily irradiation.

These quantities are said valid if they are computed with at least 60 % of valid daily irradiation. It means that

- 5-days irradiations are made from at least 3 daily estimates (60 %),

- 10-days irradiations are made from at least 6 daily estimates (60 %),

- monthly means of daily irradiation are made from at least 18 daily estimates (60 %).

Library: map_lib.c (procedures calcul_Gh and calcul_Gd)

11.   Solving the specific case of sun glitter on the ocean

The pattern of dancing highlights caused by the reflection of the sun from a water surface is called the sun glitter pattern. The surface of the ocean may be differentiated into small, mirror like facets. At spacecraft altitude, the reflecting facets will not be individually resolved. Therefore, the apparent radiance of the sea surface in any direction will depend on the fraction of the area having the proper slope for specular reflection. The observed glitter pattern shows a radiance decreasing smoothly outward from its centre, since greater and therefore less frequent slopes are required as the distance from the centre increases. As the surface roughness increases with sea state, the pattern broadens and the level of radiance at the centre decreases (Wald, Monget 1983a).

Contrary to the usual case of ground reflectance, the reflectance of the sea is highly variable during a day, ranging from null values to values greater than cloud reflectances (Wald, Monget 1983b). The approach adopted to assess the ground albedo is not effective in the case of the glitter pattern. The glitter pattern is centred on the specular point that is approximately defined as the pixel for which the satellite viewing and solar zenithal angles are equal and the difference of the azimuths of the sun and the satellite is equal to 180 ° (they are opposite). Far from the specular point, the ocean reflectance is approximately constant and the ground albedo approach is suitable.

Figure 3 exhibits the image acquired in the visible band by the Meteosat satellite. Visible in the middle of the image is the glitter pattern, a circle like shape in this case. The sun is at its zenith; the specular point is roughly southward of the nadir of the satellite.
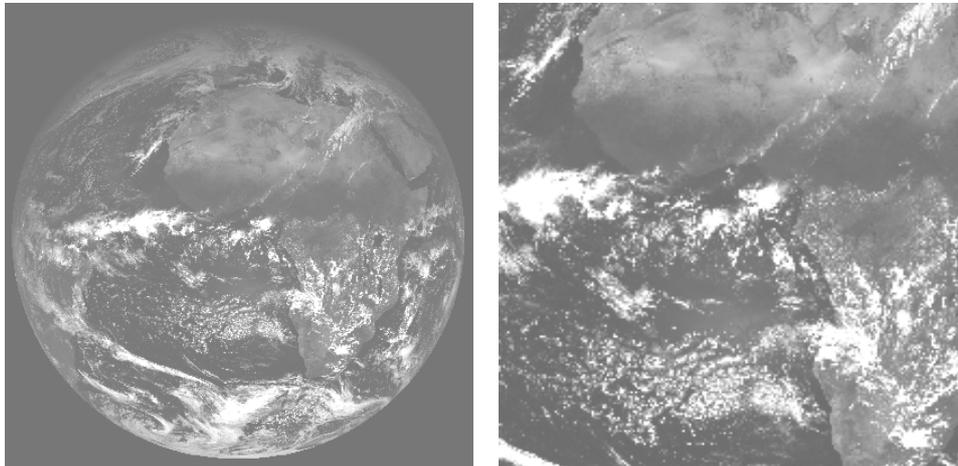

Figure 3. Meteosat visible image, taken on 1/1/1994, slot 23. Reflectances increase from black to white. The satellite is located above the Gulf of Guinea. Note the circular clear pattern in this Gulf, at the centre of the image, partly covered by clouds. The Gulf is magnified on the right image.

Within the glitter pattern, another approach should be designed to take into account the fact that the reflectance may be greater than that of a cloud. For practical reasons, it was decided to correct the cloud index in the glitter pattern instead of the reflectance.

A window is defined centred on the specular point. This point is defined as the pixel of the image for which the satellite viewing and sun zenithal angles are the closest and the difference of the azimuths of the sun and the satellite is the closest to 180 °. The search is performed between the latitudes 30 °N and –30° S approximately. The satellite viewing and zenithal angles should be greater than 40 °. Otherwise, no correction is applied. The window is large enough to encompass the largest size of the

glitter pattern: approximately 2000 km in radius. Only are considered the pixels known as belonging to the ocean. For each of these pixels, if the cloud index is greater than 0.2 (K_{ch} less than 0.8), the sky is said cloudy and no correction is applied. Otherwise, a new window of 3 x 3 pixels is defined centred on the current pixel. One counts the number of pixels exhibiting cloud indices less than 0.2. If this number is strictly greater than 5 (60 % of the total), the current pixel is considered as cloud-free and the cloud index is set to 0.

Figure 4 shows the application of the method on the previous image (Fig. 3). The uncorrected map exhibits cloud indices that are too high in the glitter pattern. They are mistaken as clouds and the resulting irradiation will be too low. Once corrected, the cloud indices offer values that are similar to the other cloudless parts of the ocean. The clouds are not affected by the corrections.
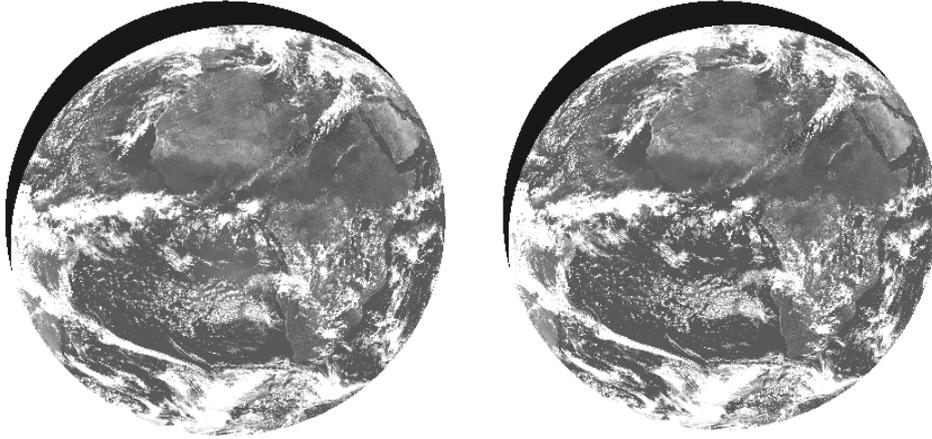

Figure 4. Map of the cloud index. Left: not corrected for the glitter effects. Note that the glitter pattern is clearly visible. Right: corrected.

Library: glitter_lib.c

12. <u>Calibration of images</u>

Meteosat images should be calibrated in radiance for the correct application of the method Heliosat-II. There are two mains sources for this information, both in agreement (Rigollier *et al.* 2002).

12.1. Calibration coefficients from HelioClim

There are three calibration coefficients

- a^t, a gain for day t,
- b^t, the offset, that is the radiance measured when viewing darkness,
- CN^t_{dark}, the digital count for the dark.

The calibration coefficients are obtained through the web site HelioClim (see online at *http://www.helioclim.org*). These coefficients are given for every day. The following figure shows an extract of the answer to the query for day 155 to day 159 of the year 1997.

The radiance L measured by the sensor is given by:

$L^t = a^t (DC^t - CN^t_{dark}) + b^t, \text{ with } L^t >= 0$

where DC^t is the digital count at t and at a given pixel. The radiance obtained is in W m^{-2} sr^{-1}.

12.2. Calibration coefficients from Eumetsat

Calibration coefficients are available on the Eumetsat Web site (Govaerts *et al.* 1998). Launch *http://www.eumetsat.de*, then click on "Data, Products and Services" (on the left), then "Meteorological Product Extraction and Distribution Service" (on the left), then "Calibration, gain settings and spectral responses", then "Meteosat VIS channel calibration".

Several couples of coefficients are provided as shown in the table below, extracted from the Eumetsat Web site. The equation for the radiance L is

$L = cs (DC - DC0)$

where cs is a gain and $DC0$ is the space count, that is the digital count observed when viewing the space. The radiance obtained is in W m^{-2} sr^{-1}.
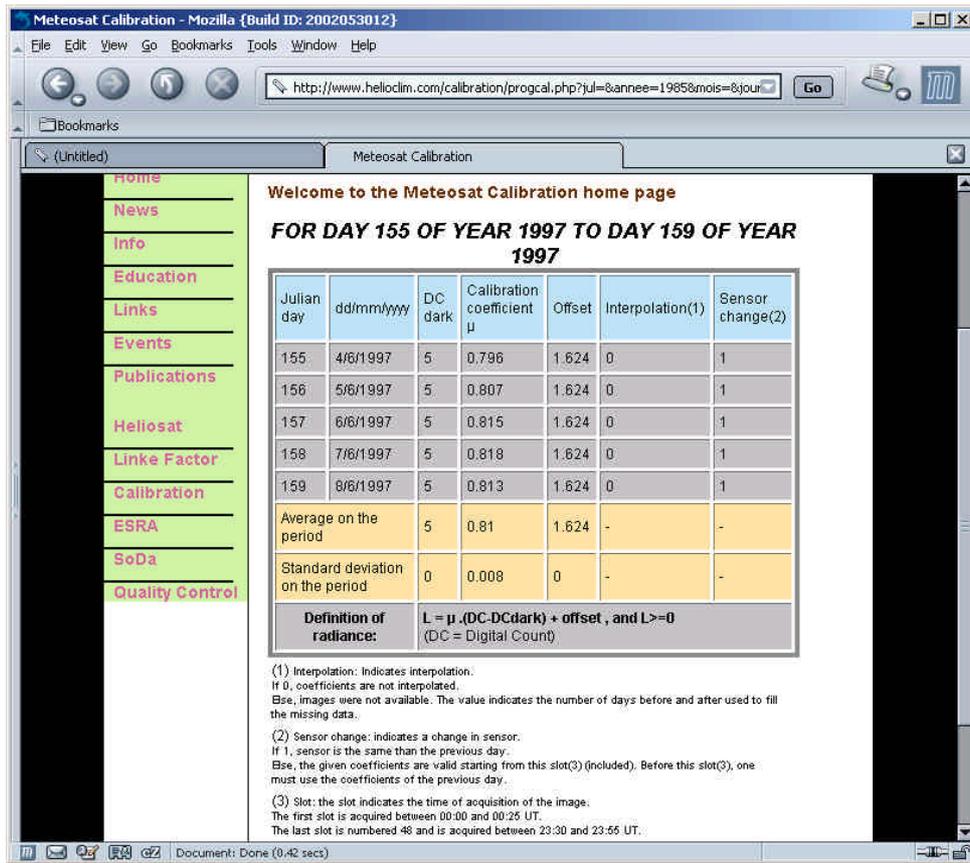
Example of the outputs of the calibration section of the Web site HelioClim

Period	Slots	Meteosat	# Obs.	Coeff.	Std. Dev.	Space Count
Jan. 1995 to Dec. 1995	24	5	489	0.857	0.0422	4.7
Jan. 1996 to Dec 1996	24	5	500	0.873	0.0330	4.7
Mar. 1997 to Dec. 1997	24	6	423	0.862	0.0379	5.7
Jan. 1998 to May 1998	17,24,28	6	542	0.860	0.0477	5.6
July 1998	12,14,18,22,24, 28,30,32,34	7	418	0.873	0.0563	5.0

Calibration coefficients in W m $^{-2}$ sr $^{-1}$/count and its associated standard deviation (from Eumetsat Web site)

13. Elevation and Linke turbidity factor

These two parameters are necessary in the execution of the method Heliosat-II. They are used in several instants of the execution. They can be obtained through the Web site SoDa for a given geographical site. It is highly recommended to download the files *tbase.zip* for elevation and *tl.zip* for the twelve months of the Linke turbidity factor, to ensure an efficient execution of the method.

The data are stored as images in raw format. One cell is one value. There is one image per month for the Linke turbidity factor. The coverage is the whole Earth, the grid is in latitude and longitude. The grid cell is squared; its size is 1/12 of degree, that is 5' of arc angle. There are 2160 rows and 4320 columns.

The upper left corner is latitude 90 N and longitude 180 W. The row increases towards South and the longitude increases towards East.

Listings of procedure for reading these files are given below. They are written in PHP. Because they are mostly composed of I/O routines, they should be re-written according to the operating system and programming language.

13.1. Elevation

The elevation database originates from the TerrainBase database (1995). The following changes were made. The value 0 means "ocean" (water body). There is no value lower than 0 m. The depressions are set to 1 m. Accordingly 1 m is the smallest value found on land.

Listing of the procedure getalt.php (the symbol // denotes comments)

```
<?
// getalt.php
// looks inside tbase file to extract altitude of a given point
// input are $lat and $lon in decimal degrees
// check if lat. and lon. are filled in. Otherwise, put 45 N and 0 E
if (empty($lat)) $lat = 45.0;
if (empty($lon)) $lon = 0.0;
// check lat. and lon. values
if ($lon > 180) $lon = 180;
if ($lon < -180) $lon = -180;
if ($lat > 90) $lat = 90;
if ($lat < -90) $lat = -90;
// compute cell position
$x = floor(($lon+180)*12);
$y = floor((90-$lat)*12);
// number of bytes to skip
$skp = 2*($y*4320+$x);
$fid = fopen("tbase.bin","r"); // open file
$bid = fseek($fid,$skp);
```

```
$lb = ord(fgetc($fid)); // there are two bytes per value
```

```
$hb = ord(fgetc($fid)); // lb is least significant byte, hb most significant byte
```

```
fclose($fid);
```

```
//print("Hb: $hb    Lb: $lb   ");
```

```
if ($hb > 127) $hb = $hb-256;
```

```
$alt = $lb+$hb*256;
```

```
printf("%d\n",$alt);
```

```
?>
```

13.2. Linke turbidity factor

The maps of the Linke turbidity factor were computed by the SoDa project. They result from the fusion of ground measurements and gridded data derived from satellite (clear sky radiances, water vapour) or not (elevation) (Remund *et al.* 2003, Lefèvre *et al.* 2003). Root mean square error is 0.7.

Note that the TL values are multiplied by 20 for their storage on one byte in the image.

Listing of the procedure getlinke.php (the symbol // denotes comments)

```
<?
```

```
// getlinke.php
```

```
// looks inside tl file to extract Tl profiles of a given point
```

```
// input are $lat and $lon in decimal degrees
```

```
// check if lat. and lon. are filled in. Otherwise, put 45 N and 0 E
```

```
if (empty($lat)) $lat = 45.0;
```

```
if (empty($lon)) $lon = 0.0;
```

```
// check lat. and lon. values
```

```
if ($lon > 180) $lon = 180;
```

```
if ($lon < -180) $lon = -180;
```

```
if ($lat > 90) $lat = 90;
```

```
if ($lat < -90) $lat = -90;
```

```
// Pixel position on the file, beginning to 0
```

```
$x = floor(($lon+180)*12);
```

```
$y = floor((90-$lat)*12);
```

```
// Number of bytes to skip to reach cell position (1 byte per value)
```

```
$skp = $y*4320+$x;
```

```
$month = array("jan","feb","mar","apr","may","jun","jul","aug","sep","oct","nov","dec");
```

```
for ($i = 0; $i < 12; $i++)
```

```
{
```

```
  $fnm = sprintf("TL5_%s.bin",$month[$i]);
```

```
  $fid = fopen($fnm,"r"); // open the file for the month $i+1
```

```
 $bid = fseek($fid,$skp);
 $pix = fgetc($fid);
 fclose($fid);
 $tl = ord($pix)/20.0; // TL values are stored with a factor 20
 printf("%.1f ",$tl);
}
printf("\n");
?>
```

```
 $bid = fseek($fid,$skp);
 $pix = fgetc($fid);
 fclose($fid);
 $tl = ord($pix)/20.0; // TL values are stored with a factor 20
 printf("%.1f ",$tl);
```

14. <u>References</u>

Angles J., Menard L., Bauer O., Wald L., 1998, A Web server for accessing a database on solar radiation parameters. In Proceedings of the Earth Observation & Geo-Spatial Web and Internet Workshop '98, Josef Strobl & Clive Best Eds., Salzburger Geographische Materialien, Universität Salzburg, Salzburg, Austria, Heft 27, 33-34.

Angles J., Menard L., Bauer O., Rigollier C., Wald L., 1999, A climatological database of the Linke turbidity factor. In Proceedings of the ISES Solar World Congress 1999, Jerusalem, Israel, July 4-9, 1999, volume I, 432-434.

Anonymous, 1996, *The Meteosat Archive, Format Guide No. 3, ISCCP Data Set (IDS) in OpenMTP Format*, February 1996, EUM FG3, Rev. 1.0, Published by Eumetsat, Darmstadt, Germany.

Bauer O., 1996, Les échanges océan-atmosphère dans l'Atlantique subtropical nord-est : apports de Meteosat. Thèse de Doctorat, Université de Nice - Sophia Antipolis, 162 p.

Beyer H.G., Costanzo C., Heinemann D., 1996, Modifications of the Heliosat procedure for irradiance estimates from satellite images. *Solar Energy*, **56**, 3, 207-212.

Beyer H. G., Reise C. and Wald L., 1992. Utilization of satellite data for the assessment of large scale PV grid integration. In *Proceedings of 11th Photovoltaic Solar Energy Conference*, pp. 1309-1312, Hardwood Academic Publ., Switzerland.

Beyer H.G., Wald L., 1996, Merging ground-measurements and satellite-derived data for the construction of global radiation map. In Proceedings of the conference « Fusion of Earth data: merging point measurements, raster maps, and remotely sensed images », Cannes, France, February 6-8, 1996, Thierry Ranchin and Lucien Wald Editors, published by SEE/URISCA, Nice, France, 37-43.

Beyer H.-G., Czeplak G., Terzenbach U., Wald L., 1997, Assessment of the method used to construct clearness index maps for the new European solar radiation atlas (ESRA). *Solar Energy*, 61, 6, 389-397.

Cano D., 1982, Etude de l'ennuagement par analyse de séquences d'images de satellite. Application à l'évaluation du rayonnement solaire global au sol. Thèse de Doctorat, École Nationale Supérieure des Télécommunications, Paris, France.

Cano D., Monget J.M., Albuisson M., Guillard H., Regas N., and Wald L., 1986, A method for the determination of the global solar radiation from meteorological satellite data, *Solar Energy*, **37**, 31-39.

CERES, 1999. Clouds and the Earth's Radiant Energy System. CD-ROM, CERES ES-4 & ES-9, available at NASA Langley Distributed Active Archive Center, Hampton, Virginia, USA. *http://asd-www.larc.nasa.gov/ceres/ASDceres.html*

Colle S., Luna de Abreu S., Couto P., Mantelli S., 1999, Distribution of solar irradiation in Brazil derived from geostationary satellite data, In Proceedings of the Solar World Congress ISES 1999 (CD-ROM), Jerusalem, July 4-9 1999.

Costanzo C., 1994, Bestimmung der solaren Einstrahlung am Boden aus Meteosat-Daten-Untersuchung und Erweiterung einer empirischen Methode. Diploma thesis, Physic Dept., Carl von Ossietzky University, Oldenburg, Germany.

Delorme C., and Gallo A., and Olivieri J., 1992, Quick use of Wefax images from Meteosat to determine daily solar radiation in France, *Solar Energy*, **49** (3), 191-197.

Diabaté L., 1989, Détermination du rayonnement solaire à l'aide d'images satellitaires. Thèse de Doctorat en Sciences, École Nationale Supérieure des Mines de Paris, Paris, France.

Diabaté L., Demarcq H., Michaud-Regas N., Wald L., 1988a, Estimating incident solar radiation at the surface from images of the Earth transmitted by geostationary satellites: the Heliosat Project, *International Journal of Solar Energy*, **5**, 261-278.

Diabaté L., Moussu G., Wald L., 1988b, An operational tool for the fine-scale mapping of the incident solar radiation using satellite images : the Heliosat station. In : Proceedings of the 1988 annual meeting of the American Solar Energy Society, pp. 11-17.

Diabaté L., Moussu G., Wald L., 1989, Description of an operational tool for determining global solar radiation at ground using geostationary satellite images, *Solar Energy*, **42**, 201-207.

Diabaté L., Michaud-Regas N., Wald L., 1989, Mapping the ground albedo of Western Africa and its time evolution during 1984 using Meteosat visible data, *Remote Sensing of Environment*, 27, 3, 211-222.

DLR – DFD (The German Remote Sensing Center. *http://www.dfd.dlr.de/*

Dogniaux R., Lemoine M., 1983, Classification of radiation sites in terms of different indices of atmospheric transparency. In Palz W. (ed.), Solar Energy R&D in the European Community, Series F, Vol. 2, Solar Energy Data. D. Reidel Publ. Co., Dordecht, 94-107.

Dumortier D., 1995, Modelling global and diffuse horizontal irradiances under cloudless skies with different turbidities. Final report JOU2-CT92-0144, Daylight II, Ecole Nationale des Travaux Publics de l'Etat, France.

Earth observation by Meteosat, 1993. Six years of observation of the Earth and its environment by Meteosat, January 1986 – December 1991, CD-ROM, available at European Space Agency, Paris, France.

EEA-EIONET. *http://www.eionet.eu.int/*

Environment Canada. Canadian Climate and Water Information. *http://www.msc-smc.ec.gc.ca/climate/index_e.cfm*

ESRA, *European Solar Radiation Atlas*, 1984. Second and Extended Edition, Vols I et II. Edited by Palz W., Commission of the European Communities, DG Science, Research and Development, Report N° EUR 9344, Brussels, Belgium.

ESRA, *European Solar Radiation Atlas*, 2000. Fourth edition, includ. CD-ROM. Edited by J. Greif, K. Scharmer. Scientific advisors: R. Dogniaux, J. K. Page. Authors: L. Wald, M. Albuisson, G. Czeplak, B. Bourges, R. Aguiar, H. Lund, A. Joukoff, U. Terzenbach, H. G. Beyer, E. P. Borisenko. Published for the Commission of the European Communities by Presses de l'Ecole, Ecole des Mines de Paris, Paris, France.

EUMETNET-European Climate Data Set, 2001. CD-ROM, version 1, November 2001, available at KNMI, The Netherlands.

Fontoynont M., Dumortier D., Heinemann D., Hammer A., Olseth J.A., Skarveit A., Ineichen P., Reise C., Page J., Roche L., Beyer H.G., Wald L., 1997, Satel-Light, Processing of Meteosat data for the production of high quality daylight and solar radiation data available on a World Wide Web Internet server, Mid-term progress report JOR3 - CT 95 - 0041, Project Satel-Light, for the Commission of the European Communities, Ecole Nationale des Travaux Publics de l'Etat, Vaulx-en-Velin, France.

Geiger M., Diabaté L., Ménard L., Wald L., 2003, A web service for controlling the quality of measurements of global solar irradiation. *To be published by Solar Energy*.

Global Daily Summary, 1994. Temperature and precipitation 1977 – 1991. CD-ROM, version 1, March 1994, available at NOAA National Climatic Data Center, Asheville, NC, USA.

Global-Land 1-km AVHRR. Vegetation Index June 21-30, 1992. CD-ROM available at Land Processes Distributed Active Archive Center, EROS Data Center, Sioux Falls, South Dakota, USA.

Global Upper Air Climatic Atlas, 1993. CD-ROM, version 1.0, April 1993, vol. 1: 1980 – 1987, vol. 2: 1985 – 1991, available at NOAA National Climatic Data Center, Asheville, NC, USA.

Govaerts, Y. M., 1999: Correction of the Meteosat-5 and –6 radiometer solar channel spectral response with the Meteosat-7 sensor spectral characteristics. *Int. J. Remote Sensing*, **20**, 3677-3682.

Govaerts, Y. M., Pinty, B., Verstraete, M. M., and J. Schmetz, 1998: Exploitation of angular signatures to calibrate geostationary satellite solar channels. *In* Proceedings of the IGARSS'98 Conference, 6-10 July1998, Seattle, USA, **1**, 327-329.

Grüter W., Guillard H., Möser W., Monget J.M., Palz W., Raschke E., Reinhardt R.E., Schwarzmann P., Wald L., 1986, Solar Radiation Data from Satellite Images, Solar Energy R&D in the European Community, Series F, Volume 4, D. Reidel Publishing Company, 100 p.

Hammer A., Heinemann D., Westerhellweg A., 1997a, Normalisation of Meteosat counts - an investigation basing on ocean pixels, Satel-Light project for the Commission of the European Communities. Carl von Ossietzky University, Oldenburg, Germany.

Hammer A., Degner T, Heinemann D., Westerhellweg A., 1997b, Modifications of the Heliosat method: cloud index improvements, detection of snow cover and results of radiative transfer calculations, Satel-Light project for the Commission of the European Communities. Carl von Ossietzky University, Oldenburg, Germany.

Hay J.E., 1981, The mesoscale distribution of solar radiation at the Earth's surface and the ability of satellites to resolve it, In Proceedings of the First Workshop on Terrestrial Solar Resource Forecasting and on Use of Satellites for Terrestrial Solar Resource Assessment, Washington D.C., February 2-5 1981.

Hay J.E., 1984, An assessment of the mesoscale variability of solar radiation at the Earth's surface, *Solar Energy*, **32**, 425-434.

Hay J.E., Hanson K.J., 1985, Evaluating the solar resource: a review of problems resulting from temporal, spatial and angular variations, *Solar Energy*, **34**, 151-161.

Heidt F.D., Teichmann C., Büchler P., Schulze-Kegel D., 1998, Satellite-based solar radiation data go Internet, In Proceedings of the second ISES-Europe Solar Congress, EuroSun'98.

HelioClim. *http://www.helioclim.org*

Hulme M., Conway D., Jones P.D., Jiang T., Barrow E.M., Turney C., 1995, A 1961-90 climatology for Europe for climate change modelling and impact applications, *International Journal of Climatology*, **15**, 1333-1363.

Iehlé A., Lefèvre M., Bauer O., Martinoli M., and Wald L., 1997, Meteosat: A valuable tool for agro-meteorology, Final report for the European Commission, Joint Research Centre, Ispra, Italy.

IFREMER-SISMER. *http://www.ifremer.fr/sismer/*

Ineichen P., Perez R., 2000, Derivation of cloud index from geostationary satellites and application to the production of solar irradiance and daylight illuminance data, *Theoretical and Applied Climatology*, **64**, 119-130.

INFEO. Information on Earth Observation. *http://www.infeo.org/*

IPCC Data Distribution Centre (International Panel on Climate Change). Providing Climate Change and Related Scenarios for Impact Assessments. CD-ROM, version 1, April 1999, available at IPCC Secretariat, Geneva. *http://ipcc-ddc.cru.uea.ac.uk*

ISCCP. International Satellite Cloud Climatology Project Data. Monthly Cloud Products: July 1983 – December 1988 and January 1989 – December 1993. CD-ROM ISCCP D2, available at NASA Langley Distributed Active Archive Center, Hampton, Virginia, USA. *http://www.cira.colostate.edu/climate/isccp/jisccp2/jisccp2.htm*

ISLCP. International Satellite Land Surface Climatology Project. Global Data Sets for Land-Atmosphere Models. CD-ROM, vols 1-5: 1987 – 1988, March 1995, available at NASA DAAC Goddard Space Flight Center, Maryland, USA.

Kasten F., 1996, The Linke turbidity factor based on improved values of the integral Rayleigh optical thickness. *Solar Energy*, **56**, 239-244.

Kasten F., 1990, Höhenabhängigkeit der Globalstrahlung bei wolkenlosem Himmel, personal communication between Kasten F., DWD, and Zelenka A., Swiss Meteorological Institute.

Kasten F. and Young A.T., 1989, Revised optical air mass tables and approximation formula. *Applied Optics*, **28** (22), 4735-4738.

Kneizys F. X., Abreu L.W., Anderson G.P., Chetwynd J.H., Shettle E.P., Berk A., Bernstein L.S., Robertson D.C., Acharya P., Rothman L.S., Selby J.E.A., Galery W.O., Cough S.A., 1996, The MODTRAN 2 / 3 Report and LOWTRAN 7 Model. Technical report, Phillips Laboratory, Geophysics Directorate, Hanscom AFB.

Lefèvre M., Bauer O., Iehlé A., Wald L., 2000, An automatic method for the calibration of time-series of Meteosat images, *International Journal of Remote Sensing*, **21** (5), 1025-1045.

Lefèvre M., Remund J., Albuisson M., Wald L., 2002, Study of effective distances for interpolation schemes in meteorology. European Geophysical Society, 27th General Assembly, Geophysical Research Abstracts, vol. 4, April 2002, EGS02-A-03429.

Lefèvre M., Remund J., Albuisson M., Ranchin T., Wald L., 2003, Fusing ground measurements and satellite-derived products for the construction of climatological maps in atmosphere optics. To be presented at the EARSeL 23rd Annual Symposium, June 2-5, Gent, Belgium.

Lefèvre M., Rigollier C., Cros S., Wald L., 2002, Toward a solar climatological database: the HelioClim project. In Proceedings, EARSeL Symposium 2002.

Lefèvre M., Rigollier C., Cros S., Albuisson M., Wald L., 2002, A shortwave radiation database to support GODAE-related activities. Proceedings of the International Symposium "En route to GODAE", 13-15 June 2002, Biarritz, France. Published by CNES, Toulouse, France, 2002, pp. 157-158.

Maxwell E. L., 1998, Metstat - The solar radiation model used in the production of the national solar radiation data base (NSRDB), *Solar Energy*, 62(4), 263-279.

MedAtlas. *http://www.meteo.ru/nodc/project/project.htm*

Medias-France, 1994. Mediterranean Oceanic Database – Satellite data and meteorological model outputs. CD-ROM, available at Medias-France, Toulouse, France.

Meteonorm, 1997, Remund J., Kunz S., *Meteonorm version 3.0, Global meteorological database for solar energy and applied climatology*, Nova Energie GmbH, Schachenallee 29, CH-5000 Aarau, Switzerland.

Meteonorm, 2000, Remund J., Kunz S., Lang R., *Meteonorm version 4.0, Global meteorological database for solar energy and applied climatology*, Nova Energie GmbH, Schachenallee 29, CH-5000 Aarau, Switzerland.

Meteosat Collection. CD-ROMs available at European Space Agency, Paris, France.

Michaud-Regas N., 1986, Mise en oeuvre et validation d'une méthode opérationnelle et automatique pour l'évaluation d'atlas solaires en Europe à l'aide de mesures satellitaires Meteosat. Thèse de Doctorat, Université Paris VII, Paris, France.

MODB (The Mediterranean Oceanic Database). *http://modb.oce.ulg.ac.be/*

Molineaux B., Ineichen P., Delauney J.J., 1995, Direct luminous efficacy and atmospheric turbidity – improving model performance, *Solar Energy*, **55** (2), 125-137.

Möser W., Raschke E., 1983, Mapping of global radiation and of cloudiness from Meteosat image data: theory and ground truth comparisons, *Meteorologische Rundschau*, **36**, 33-41.

Möser W., Raschke E., 1984, Incident solar radiation over Europe estimated from Meteosat data, *Journal of Applied Meteorology*, **23**, 166-170.

Moussu G., Diabaté L., Obrecht D., Wald L., 1989, A method for the mapping of the apparent ground brightness using visible images from geostationary satellites, *International Journal of Remote Sensing*, **10** (7), 1207-1225.

NASA-EO Newsroom. *http://earthobservatory.nasa.gov/Newsroom/NewImages/*

NASA-EOSDIS (Earth Observing System Data and Information System). *http://eospso.gsfc.nasa.gov/eos_homepage/scientists.html*

NASA-JPL DAAC. Physical Oceanography Distributed Active Archive Center. *http://podaac.jpl.nasa.gov/*

NASA-LARC. Live Access to Climate Data. *http://asd-www.larc.nasa.gov/cgi-bin/climate_server*

NASA-LARC. Surface Meteorology and Solar Energy Data Set. *http://eosweb.larc.nasa.gov/sse/*

NASA-SAGE. Stratospheric Aerosol Measurement II: October 1978 – January 1993. CD-ROM, available at NASA Langley Distributed Active Archive Center, Hampton, Virginia, USA.

NASA-SRB. First WCRP Surface Radiation Budget Global Data Sets. Shortwave Radiation Parameters March 1985 – December 1988. CD-ROM, version 1.1, available at NASA Langley Distributed Active Archive Center, Hampton, Virginia, USA.

NASA Web site for Atmospheric Chemistry and Solar Radiation. *http://www.earth.nasa.gov/science/Science_atmosphere.html*

Neckel, H., and D. Labs, 1984, The solar radiation between 3300 and 12500 Å. *Solar Physics*, 90, 205-258.

NOAA – NCDC. *http://lwf.ncdc.noaa.gov/oa/ncdc.html*

NREL (National Renewable Energy Laboratory). Solar Radiation Resource Information. *http://rredc.nrel.gov/solar/*

Obrecht D., 1990, Météorologie solaire et images satellitaires : cartographie du rayonnement solaire, détermination de l'albédo des sols et évaluation de l'ennuagement. Thèse de Doctorat en Sciences, Université de Nice- Sophia Antipolis, France.

Pastre C., 1981, Développement d'une méthode de détermination du rayonnement solaire global à partir des données Meteosat, *La Météorologie*, VIᵉ série N°24, mars 1981.

Perez R., Seals R., Zelenka A., 1997, Comparing satellite remote sensing and ground network measurements for the production of site/time specific irradiance data, *Solar Energy*, **60**, 89-96.

Perrin de Brichambaut C., Vauge C., 1982, *Le gisement solaire : Evaluation de la ressource énergétique*, Paris: Technique et documentation (Lavoisier).

Pinker R. T. and Laszlo I., 1991. Effects of spatial sampling of satellite data on derived surface solar irradiance. *Journal of Atmospheric and Oceanic Technology*, **8**, 1, 96-107.

Raschke E., Stuhlmann R., Palz W., Steemers T.C., 1991, *Solar Radiation Atlas of Afric*a. Published for the Commission of the European Communities by A. Balkema, Rotterdam, 155 p.

Remund J., Page J., 2002, Advanced parameters. Chain of algorithms: short- and longwave radiation with associated temperature prediction resources. Report to the European Commission, SoDa (Integration and exploitation of networked Solar radiation Databases for environment monitoring) project IST-1999-12245, 72 p. (see online at *http://soda.jrc.it*).

Remund J., Wald L., Lefevre M., Ranchin T., Page J., 2003, Worldwide Linke turbidity information. To be presented at the ISES Annual Conference, Göteborg, Sweden.

RETScreen. *http://retscreen.gc.ca/*

Rigollier C., 2000, Vers un accès à une climatologie du rayonnement solaire : estimation de l'irradiation globale à partir d'images satellitales. Thèse de Doctorat en Sciences et Technologies de l'Information et de la Communication, Université Nice – Sophia Antipolis, France, 194 p.

Rigollier C., Bauer O., Wald L., 2000, On the clear sky model of the 4th European Solar Radiation Atlas with respect to the Heliosat method, *Solar Energy*, **68** (1), 33-48.

Rigollier C., Lefèvre M., Blanc Ph., Wald L., 2002. The operational calibration of images taken in the visible channel of the Meteosat-series of satellites. *Journal of Atmospheric and Oceanic Technology*, 19(9), 1285-1293.

Rigollier C., Wald L., 1999, The HelioClim Project: from satellite images to solar radiation maps. In *Proceedings of the ISES Solar World Congress 1999*, Jerusalem, Israel, July 4-9, 1999, volume I, pp 427-431.

Rigollier C., Wald L., 1999. Towards operational mapping of solar radiation from Meteosat images. In Proceedings, EARSeL Symposium 1998 "operational remote sensing for sustainable development", Enschede, The Netherlands, Nieuwenhuis G., Vaughan R., Molenaar M. eds, Balkema, Rotterdam, pp 385-391.

Rigollier C., Wald L., 2000. Selecting a clear-sky model to accurately map solar radiation from satellite images. In : Proceedings, EARSeL Symposium 1999 "remote sensing in the 21st Century: economic and environmental applications", Valladolid, Spain, Casanova J.-L., Vaughan R. eds, Balkema, Rotterdam, pp 131-137.

Satel-Light. *http://www.satel-light.com/*

Schiffer, R.A. and Rossow, W.B., 1983, The International Satellite Cloud Climatology Project (ISCCP): The first project of the World Climate Research Programme. *Bulletin American Meteorological Society*, 64, 779-784.

Schiffer, R.A. and Rossow, W.B., 1985, ISCCP global radiance data set: A new resource for climate research. *Bulletin American Meteorological Society*, 66, 1498-1503.

Stuhlmann R., Rieland M., Raschke E., 1990, An improvement of the IGMK model to derive total and diffuse solar radiation at the surface from satellite data, *Journal of Applied Meteorology*, **29**, 596-603.

Supit I., 1994, Global radiation. Agriculture series, EUR 15745, European Commission, Office for Official Publications, Luxembourg, 194 p.

SWERA. Solar and Wind Resource Assessment. *http://swera.unep.net/*

SWITCH. Solar Water Integrated Thermal Cooling and Heating Systems. *http://fernande.cma.fr/switch/*

Tanré D., Deroo C., Duhaut P., Herman M., Morcrette J.J., Perbos J., Deschamps P.Y., 1990, Description of a computer code to simulate the satellite signal in the solar spectrum: the 5S code, *International Journal of Remote Sensing*, 11(4), 659-668.

Taylor V.R., Stowe L.L., 1984a, Reflectance characteristics of uniform Earth and cloud surfaces derived from Nimbus 7 ERB, *Journal of Geophysical Research*, **89**(D4), 4987-4996.

Taylor V.R., Stowe L.L., 1984b, Atlas of reflectance patterns for uniform Earth and cloud surfaces (Nimbus 7 ERB – 61 days), NOAA Technical Report NESDIS 10, July 1984, Washington, DC, USA.

TerrainBase, Worldwide Digital Terrain Data, 1995. Documentation Manual, CD-ROM Release 1.0, April 1995. NOAA, National Geophysical Data Center, Boulder, Colorado, USA.

Unidata. *http://www.unidata.ucar.edu/*

USGS (United States Geological Survey). http://www.usgs.gov/

Vermote E., Tanré D., Deuzé J.L., Herman M., Morcrette J.J., 1994, Second Simulation of the Satellite Signal in the Solar Spectrum (6S), 6S User Guide, NASA-Goddard Space Flight Center - Code 923, Greenbelt, USA.

Wald L., Albuisson M., Best C., Delamare C., Dumortier D., Gaboardi E., Hammer A., Heinemann D., Kift R., Kunz S., Lefèvre M., Leroy S., Martinoli M., Ménard L., Page J., Prager T., Ratto C., Reise C., Remund J., Rimoczi-Paal A., Van der Goot E., Vanroy F., and Webb A., 2002, SoDa: a project for the integration and exploitation of networked solar radiation databases. In: Environmental Communication in the Information Society, W. Pillmann, K. Tochtermann Eds, Part 2, pp. 713-720. Published by the International Society for Environmental Protection, Vienna, Austria.

Wald L., Monget J.M., 1983a, Sea surface winds from sun glitter observations. *Journal of Geophysical Research*, 88, C4, 2547-2555.

Wald L., Monget J.M., 1983b, Remote sensing of the sea-state using the 0.8-1.1 microns channel. *International Journal of Remote Sensing*, 4, 2, 433-446, 1983. Comments by P. Koepke and reply, 6, 5, 787-799, 1985.

Wald L., Wald J.-L., Moussu G., 1992, A technical note on a low-cost high-quality system for the acquisition and digital processing of images of WEFAX type provided by meteorological geostationary satellites. *International Journal of Remote Sensing*, 13, 5, 911-916.

World Meteorological Organization (WMO), 1981, Meteorological aspects of the utilization of solar radiation as an energy source. Annex: World maps of relative global radiation. Technical Note N° 172, WMO-N° 557, Geneva, Switzerland, 298 pp.

WMO-CLINO, 1998. Global Climate Normals (CLINO) 1961 – 1990. CD-ROM, version 1, November 1998, available NOAA National Climatic Data Center, Asheville, NC, USA.

WMO Online Satellite Imagery Sites. *http://www.wmo.ch/hinsman/imagery.html*

WMO – World Radiation Data Center. *http://wrdc.mgo.rssi.ru/Lefts_en.htm*

Zelenka A., Czeplak G., d'Agostino V., Josefson W., Maxwell E., Perez R., 1992, Techniques for supplementing solar radiation network data, Technical Report, International Energy Agency, # IEA-SHCP-9D-1, Swiss Meteorological Institute, Krahbuhlstrasse, 58, CH-8044 Zurich, Switzerland.

Zelenka A., Perez R., Seals R., and Renné D., 1999, Effective accuracy of satellite-derived hourly irradiances, *Theoretical and Applied Climatology*, **62**, 199-207.